

2 3 4

5

6 7

8

9

10 11

13

14 15

16

17

18

19

20

21

22

23

24

25

26

27

28

29

30

3132

33

34

35



Global Perspectives on Nitrate Aerosol Dynamics: A Comprehensive Sensitivity Analysis

Alexandros Milousis 1 , Susanne M.C. Scholz 1 , Hendrik Fuchs 1,2 , Alexandra P. Tsimpidi 1 , and Vlassis A. Karydis 1

¹Institute of Climate and Energy Systems, ICE-3: Troposphere, Forschungszentrum Jülich GmbH, Jülich, Germany

²Department of Physics, University of Cologne, Cologne, Germany

12 Correspondence to:

Vlassis A. Karydis (v.karydis@fz-juelich.de) and Alexandra P. Tsimpidi (a.tsimpidi@fz-juelich.de)

Abstract

In recent years, nitrate aerosols have emerged as a dominant component of atmospheric composition, surpassing sulfate aerosols in both concentration and climatic impact. However, accurately simulating nitrate aerosols remains a significant challenge for global atmospheric models due to the complexity of their formation and regional variability. This study investigates key factors influencing nitrate aerosol formation to improve simulation accuracy in highly polluted regions. Using the advanced EMAC climate and chemistry model, we assess the effects of grid resolution, emission inventories, and thermodynamic, chemical, and aerosol scavenging processes. The ISORROPIA II thermodynamic model is employed to simulate the formation of inorganic aerosols. Model predictions are compared with surface observations of particulate nitrate in PM₁ and PM_{2.5} size fractions, including PM_{2.5} data from filter-based observational networks and PM₁ data from aerosol mass spectrometer field campaigns across Europe, North America, East Asia, and India. Results show that the model overestimates PM_{2.5} nitrate concentrations, especially in East Asia, with biases up to a factor of three. Increasing grid resolution, adjusting N₂O₅ hydrolysis uptake coefficient, and utilizing an appropriate emission database (e.g., CMIP6) improve performance. However, these adjustments do not necessarily enhance PM₁ predictions, which remain underestimated, especially in urban downwind sites. Seasonal variations and diurnal trends reveal discrepancies in model performance, especially in Europe and urban downwind locations. In Europe, model bias is driven by an unrealistically sharp decrease in nitrate aerosol levels from morning maxima to evening minima. Sensitivity tests show relatively small impact on total tropospheric nitrate burden, with variations within 25%.



38

39

40

41 42

43

44

45

46

47 48

49

50

51

52 53

54

55

56

57

58

59

60

61

62 63

64

65

66

67 68

69

70

71 72

73

74

75

76

77

78

79

80

81



1. Introduction

Aerosols are a critical and complex component of the Earth's climate system, due to the complexity of their chemical composition and the many changes they undergo during their atmospheric lifetime. The composition of anthropogenic aerosols, influenced by the diverse precursor gases emitted by anthropogenic activities, plays a pivotal role in shaping climate and air quality. Of particular concern are aerosols with a diameter of less than 2.5 μ m (PM_{2.5}), which have been linked to a significant global mortality rate, estimated to exceed four million deaths per year (Chowdhury et al., 2022; Im et al., 2023). Furthermore, anthropogenic aerosols have a significant impact on the Earth's energy balance by causing a net cooling effect that tends to mask the warming induced by greenhouse gases (Storelymo et al., 2016; Glantz et al., 2022; Nair et al., 2023). Among the various types of anthropogenic aerosols, sulfates (SO₄²-) have become the dominant type in terms of mass concentrations, with a tropospheric burden that is more than twice as high than that of nitrates (NO₃⁻) (Bellouin et al., 2011; Myhre et al., 2013; Karydis et al., 2016). However, numerous studies have indicated a shift in this regime, with nitrates challenging the dominance of sulfates in several key regions of the polluted northern hemisphere (Tsimpidi et al., 2024), including Europe (Lanz et al., 2010; Aksoyoglu et al., 2017), the USA (Walker et al., 2012), and East Asia (Wang et al., 2013; Li et al., 2020). This phenomenon can be attributed to the strict restrictions on sulfur dioxide (SO₂) emissions worldwide, which have not always been accompanied by a corresponding reduction in nitrogen oxide (NOx) emissions, and particularly ammonia (NH₃), which has increased in recent decades (Bellouin et al., 2011; Hauglustaine et al., 2014). Nitrate aerosols are of particular importance because they can influence atmospheric chemistry through heterogeneous reactions with dust and sea salt (Karydis et al., 2016; Kok et al., 2023), which also lead to more acidic conditions in aerosols (Karydis et al., 2021). Additionally, nitrate aerosols have been shown to affect climate through a direct radiative effect that leads to cooling (Myhre et al., 2013; Hauglustaine et al., 2014; Klingmuller et al., 2019; Milousis et al., 2025). Furthermore, nitrate aerosols influence the properties of clouds and other aerosol species, resulting in a complex indirect radiative effect (Klingmuller et al., 2020; Milousis et al., 2025). Consequently, the precise representation of nitrate aerosols in global chemistry climate models (CCM) becomes increasingly important, as they are projected to have the most substantial impact on climate and air quality by the end of the century.

However, this task presents a number of challenges. Nitrate aerosol formation is highly sensitive to the levels of its precursors (Karydis et al., 2011), therefore, their accurate representation in models is an essential starting point for realistic simulation of nitrate aerosols. Furthermore, nitrate aerosols are inherently semi-volatile, which means that partitioning between the gas and particle phases is a complicated process as equilibrium conditions must be met, which in turn complicates the calculations (Seinfeld and Pandis, 2016). To ensure the reliability of model predictions, it is imperative that they accurately represent the equilibrium between the gas and particle phases, which depends on various atmospheric conditions. Humidity and temperature have been identified as key factors in determining this equilibrium, while atmospheric acidity has been shown to play a crucial role in regulating partitioning processes (Ansari and Pandis, 2000; Guo et al., 2016; Pye et al., 2020). The complexity of the system is further increased by the interaction of nitrate aerosols with other important aerosol species, such as sea salt and mineral dust. The inclusion of these pathways can be critical for accurate predictions (Karydis et al., 2010; Karydis et al., 2016; Kakavas and Pandis, 2021). The complex nature of nitrate aerosols often leads to discrepancies between model estimates and observations, with models frequently predicting higher mass concentrations. For instance, overestimations of approximately 2 µg/m³ have been found in Europe





(Jones et al., 2021; Milousis et al., 2024), with biases reaching a factor of 5 or more in some cases (Chen et al., 2018). Analogous findings have been documented in the US (Walker et al., 2012; Zakoura and Pandis, 2018, 2019; Jones et al., 2021), while model simulations in East Asia have exhibited even greater biases (Miao et al., 2020; Milousis et al., 2024), with Xie et al. (2022) noting that approximately 60% of studies modeling particle concentrations in China overpredicted particulate nitrate levels. The potential causes of such biases can be categorized into several groups, covering a range of physicochemical processes and model characteristics.

A fundamental reason for discrepancies between model predictions and observations, as well as between predictions made by different models, is the grid resolution employed. A high spatial resolution (i.e., a substantial number of simulated grid cells with reduced size) facilitates the capture of chemical interactions that precursors undergo and their various removal processes with a high degree of precision. Conversely, a low spatial resolution may result in oversimplifications. It is important to note that the increased complexity of the representation is associated with higher computational costs. However, the use of high spatial resolution has been shown to reduce biases in predicted nitrate aerosol concentrations by 60-80% (Metzger et al., 2002; Zakoura and Pandis, 2018, 2019). Furthermore, Schaap et al. (2004) and Heald et al. (2012) note that in certain cases, the use of high resolution is essential to ensure the accurate representation of observational data by the model.

Another source of discrepancies between model and measurement results is the accuracy of the emission inventories in the model. Specifically in the case of nitrate aerosols, the presence of ammonia (NH₃) emissions is critical in determining their concentrations. In regions where there is an excess of ammonia, it forms ammonium nitrate (NH₄NO₃) after having neutralized sulfuric acid (H₂SO₄) and reacting with nitric acid (HNO₃) (Seinfeld and Pandis 2016). The main sources of NH₃ emissions are associated with agricultural activities, and the accuracy of their representation in emission inventories is not always ensured (Nair and Yu, 2020). This is due to the influence of various factors. These include the variety of agricultural practices and management techniques used, as well as the land changes induced by agricultural activities in general (Sutton et al., 2013; Ge et al., 2020). These factors make it difficult to ensure consistent accuracy regarding NH₃ emissions. Additionally, the distinct characteristics of soil types and climates across different regions can substantially influence emission factors (Reis et al., 2009; Nair and Yu, 2020), a critical consideration in the development of a global inventory. For instance, Zhang et al. (2017) have highlighted that numerous prior NH₃ emission inventories in China employed emission factors determined for Europe. In addition, the diurnal and seasonal variability of NH₃ emissions must be considered in global inventories to ensure representability (Pinder et al., 2006; Hendriks et al., 2016). These considerations are equally relevant to the representation of other precursor gases, such as NOx and SO2, which are also crucial for particulate nitrate formation (Tsimpidi et al., 2007; 2008; 2012).

The thermodynamic state of the aerosol is another factor that plays an important role in the accuracy of model predictions. Typically, thermodynamic equilibrium models can assume that the particle can only exist as a supersaturated aqueous solution throughout its lifetime (metastable conditions), or they can calculate its deliquescence into a solid state as the ambient relative humidity decreases (stable conditions). The choice of the thermodynamic state can lead to differences in the acidity of the aerosol, which, in turn, can affect the prediction of concentrations for species such as nitrate, as less acidic conditions favor its partitioning into the aerosol phase and vice versa (Nenes et al., 2020). Previous studies have examined the impact of the thermodynamic state assumption on aerosol concentration predictions and have demonstrated that the choice is





region dependent. For instance, a stable state has been shown to yield more realistic predictions when simulating arid and desert regions (Karydis et al., 2016). Furthermore, Fountoukis et al. (2009) and Karydis et al. (2010) found that stable thermodynamic conditions are more consistent with observations when the ambient relative humidity (RH) is below 50%. Conversely, Ansari and Pandis (2000) found that metastable thermodynamic conditions are more suitable for regions with intermediate relative humidity (RH) and low aerosol concentrations. However, no significant differences were observed between these two assumptions for high aerosol concentrations. Guo et al. (2016) determined that metastable thermodynamic conditions are more representative of areas exhibiting characteristics analogous to those observed in the Northeastern US. In contrast, Milousis et al. (2024) found minimal differences between the two assumptions for major inorganic pollutant concentrations (i.e., nitrate, sulfate, and ammonium aerosols, as well as mineral cations) on a global scale.

Another factor influencing model predictions of nitrate aerosols is the chemistry of dinitrogen pentoxide (N₂O₅), which is particularly important for the nocturnal production of nitrate particles. Specifically, N₂O₅, a compound derived from the oxidation of NOx species, undergoes heterogeneous hydrolysis on particle surfaces in the presence of sufficient amounts of water, resulting in the formation of HNO₃, a pivotal precursor of nitrate aerosols. This heterogeneous pathway has been shown to dominate the nighttime production of HNO₃, potentially accounting for up to 50% of particulate nitrate production in polluted areas during both winter (Liu et al., 2020) and summer (Qu et al., 2019). The hydrolysis reaction is predominantly governed by a corresponding uptake coefficient, with numerous models employing a single average value. However, the reaction exhibits a strong dependence on environmental quantities such as temperature and relative humidity. Consequently, some studies suggest the utilization of different values in models depending on the prevalent ambient conditions of the examined region. For instance, Wang et al. (2020) proposed a significantly lower value than the conventional value utilized in CCMs (0.02) to better align with conditions observed in Beijing. A similarly suggestion was made by Phillips et al. (2016) for semi-rural regions in Germany, with the intent of providing more precise estimates of particulate nitrate, and this is supported by a number of studies in various parts of the US as well (Bertram et al., 2009; Brown et al., 2009; Chang et al., 2011; Chang et al., 2016). The significance of N₂O₅ chemistry is particularly pronounced in regions exhibiting activities that contribute to elevated NOx concentrations. This effect is further exacerbated in areas characterized by intrusions of particles, such as mineral dust and/or sea salt, which facilitate heterogeneous reactions.

Furthermore, model predictions of nitrate aerosols can be strongly influenced by the model treatment of their wet deposition and, specifically, the manner in which cloud acidity affects the dissolution of HNO₃. Specifically, in less acidic conditions, elevated in-cloud dissolution of HNO₃ is observed to achieve overall electroneutrality, leading to increased particulate nitrate production (Seinfeld and Pandis, 2016; Tilgner et al., 2021). Therefore, it is essential that a model accurately represents in-cloud properties, as the pH conditions in regions with different characteristics will be more accurately captured. This, in turn, will facilitate a more comprehensive understanding of nitrate formation processes.

This study aims to investigate the sensitivity of the simulated nitrate aerosol concentration to a number of parameters on a global scale. For this purpose, the global atmospheric chemistry-climate model EMAC was used, with different configurations and parameterizations covering all the aspects mentioned above that influence the prediction of particulate nitrate concentrations. The model performance was evaluated against network and station observations of NO₃⁻ in the PM_{2.5}



177

178

179

180

181

182

183

184

185

186

187

188

189

190

191

192

193

194

195

196

197 198

199

200201

202

203

204

205

206

207

208

209

210

211

212

213

214

215

216

217



and PM₁ size ranges, with the aim of identifying the parameters that are most relevant over specific regions.

2. Methodology

2.1 Model setup

The model utilized in this study is the EMAC global chemistry and climate model (Jöckel et al., 2006). EMAC comprises a series of submodels, which are interconnected via the Modular Earth Submodel System (MESSy) (Jöckel et al., 2005) to the base (core) model, namely the fifth generation European Center Hamburg general circulation model (ECHAM5) (Roeckner et al., 2006). The gas phase chemistry is simulated by the submodel MECCA (Sander et al., 2019) with a simplified scheme similar to that used in the Chemistry Climate Model Initiative (CCMI), as described by Jöckel et al. (2016). The liquid phase chemistry is simulated by the submodel SCAV (Tost et al., 2006), which is also responsible for the wet deposition treatment of trace gases and aerosols. The submodel DRYDEP (Kerkweg et al., 2006b) addresses the dry deposition of trace gases and aerosols, while the submodel SEDI (Kerkweg et al., 2006b) handles the gravitational sedimentation of aerosols. The GMXe submodel (Pringle et al., 2010a; Pringle et al., 2010b) simulates aerosol microphysical processes and the gas-to-particle partitioning of inorganic species. For more detailed information on these particular processes, the reader is referred to Section 2.2. The ORACLE submodel (Tsimpidi et al., 2014; 2018) is responsible for simulating the composition and chemical evolution of all organic aerosol species. The microphysical processes of clouds are simulated by the CLOUD submodel (Roeckner et al., 2006), using the two-moment microphysical scheme for liquid and ice clouds of Lohmann and Ferrachat (2010), while considering a physically based treatment for the processes related to the activation of liquid droplets (Karydis et al., 2017) and ice crystals (Bacer et al., 2018). In this study, all simulations performed were nudged towards the actual meteorology using ERAI data (Dee et al., 2011), and concern the period 2009-2018, with the first year being used as the model spin-up period.

The spatial resolution used in all simulations, except for two sensitivity cases (see Section 2.3), corresponds to T63L31, which has a grid resolution of 1.875° x 1.875° and covers vertical altitudes up to 25 km, divided into 31 layers. The database of anthropogenic emissions in terms of aerosols and their precursors, utilized by all simulations with the exception of the related sensitivity cases (see Section 2.3), was derived from the CAMS inventory (Inness et al., 2019). Biomass burning emissions were taken from the GFEDv4.1 database (Randerson et al., 2017). The natural emissions of NH₃, originating from soil and oceanic volatilization, were obtained from the GEIA database (Bouwman et al., 1997). The biogenic soil emissions of NO were calculated online during runtime using the algorithm of Yienger and Levy (1995). Lightning production of NOx is also calculated online by the LNOx submodel (Tost et al., 2007a) based on the parameterization of Grewe et al. (2001). The emissions of SO₂ from volcanic eruptions are obtained from the AEROCOM database (Dentener et al., 2006). Sea salt emissions are calculated online according to the parameterization of Guelle et al. (2001), which utilizes precalculated lookup tables to determine the wind speed-dependent mass and particle number fluxes for the accumulation and coarse mode sizes, which applies for sea salt aerosols. For more detailed information on the calculation of the lookup tables, the reader is referred to Stier et al. (2005) and Kerkweg et al. (2006a). The AIRSEA submodel (Pozzer et al., 2006) calculates oceanic emissions of dimethyl sulfide (DMS) online. Additionally, dust emission fluxes are calculated online using the parameterization of Astitha et al. (2012). This method considers both the meteorological



224

225

226

227228

229

230

231

232

233

234

235

236

237

238

239

240

241

242

243

244

245

246

247

248

249

250

251

252

253

254

255

256

257

258

259

260

261

262



information of each grid cell (temperature and relative humidity) and the various friction velocity thresholds above which dust particle suspension occurs. The mineral dust composition is determined by the bulk composition, and the mineral ions Na⁺, Ca²⁺, K⁺ and Mg²⁺ are estimated as a fraction of the total dust emission flux based on the chemical composition of the soil in each grid cell (Karydis et al., 2016; Klingmüller et al., 2018).

2.2 Inorganic aerosol partitioning

In this study, all calculations related to the thermodynamics of inorganic aerosols, as well as their phase partitioning process, are performed by ISORROPIA II v2.3 (Fountoukis and Nenes, 2007), which is a thermodynamic module integrated into the GMXe submodel. ISORROPIA II v2.3 treats the chemical system of K^+ – Ca^{2+} – Mg^{2+} – NH_4^+ – Na^+ – SO_4^{2-} – NO_3^- – Cl^- – H_2O aerosols and has the ability to simulate either a stable thermodynamic state, where aerosols are allowed to precipitate into solid salts, or a metastable state, where aerosols remain in a supersaturated aqueous solution even at low relative humidities. The first case is used for the base case assumption of this study, along with all other sensitivity simulations, with the exception of one (Section 2.3). ISORROPIA II v2.3 is a slightly updated version of ISORROPIA II that concerns more accurate predictions of aerosol pH near neutral conditions (Song et al., 2018). However, this affects only a small number of calculations in the different compositional sub-regimes of ISORROPIA II. Specifically, in some cases, NH₃ evaporation was not taken into account in the aerosol pH calculations, resulting in values that approached neutrality. However, this had a negligible effect on both the predicted NH₃ and the inorganic aerosol concentrations. The ISORROPIA II v2.3 model utilizes Bromley's formula (Bromley, 1973) to calculate the binary activity coefficients for multicomponent mixtures. For specific component pairs, it employs the Kusik-Meissner relationship (Kusik and Meissner, 1978), which incorporates the temperature dependence of Meissner and Peppas (1973). Further insights can be found in Fountoukis and Nenes (2007).

In the GMXe submodel, aerosol size is described by seven lognormal size modes, four of which are assigned to a soluble fraction and the remaining three to an insoluble fraction. The soluble fraction includes the nucleation, Aitken, accumulation, and coarse size modes, while the insoluble fraction includes only the latter three (Pringle et al., 2010a, 2010b). In the aerosol partitioning process, kinetic limitations must be considered, as only sizes smaller than coarse mode can reach equilibrium within the timeframe of one model time step (10 minutes for this study). Consequently, the partitioning calculations are performed in two stages. Initially, the amount of gas phase species that can kinetically condense to the particle phase within this timeframe is calculated according to the diffusion limited condensation theory of Vignati et al. (2004). Subsequently, the partitioning between the gas and particle phases is estimated by assuming instantaneous equilibrium for all aerosol size modes, as the ISORROPIA II v2.3 routines are called separately for each one. Finally, the transfer of material between the soluble and insoluble modes is calculated by GMXe after the partitioning calculations have been completed. This transfer can occur in two ways: by coagulation, where two particles of different modes collide and the resulting particle is in the soluble mode; or if substantial soluble material has condensed onto an insoluble particle, the latter is transferred to the soluble mode (Pringle et al., 2010a, 2010b).

2.3 Sensitivity configuration details

A total of eight simulations were performed (base case and seven sensitivity cases) in an attempt to cover all aspects that influence the model predictions of particulate nitrate concentrations, as discussed in Section 1, and whose configurations are summarized in Table 1. The objective is to ascertain whether a specific configuration can most accurately reproduce the measurements of





 $PM_{2.5}$ and PM_1 concentrations in the most heavily polluted regions of the globe. The base case simulation was performed using the following combination of configurations. A T63L31 spatial resolution (1.875° x 1.875° grid) with anthropogenic emissions provided by the CAMS database is used. The aerosols' thermodynamic state was assumed to be stable, i.e., it was permitted to precipitate into solid salts at low relative humidity (RH). Aerosol scavenging is addressed by a comprehensive mechanism encompassing over 150 chemical reactions for the liquid phase, in addition to the online calculation of the in-cloud and precipitation pH (Tost et al., 2006, 2007b). The uptake coefficient of N_2O_5 hydrolysis is 0.02 according to the parameterization proposed by Evans and Jacob (2005).

In the first two sensitivity model runs (RES_low and RES_high), only the spatial grid resolution was changed. The change involved the adoption of a lower resolution, characterized by a reduction in the number of grid cells, and a higher resolution, marked by an increase in the number of grid cells. Notably, the vertical resolution was maintained at 31 layers, consistent with the base case. The lower spatial resolution is the T42L31 resolution, which corresponds to a $2.813^{\circ} \times 2.813^{\circ}$ grid and the higher spatial resolution is the T106L31 resolution, which corresponds to a $1.125^{\circ} \times 1.125^{\circ}$ grid. The other two sensitivity model runs ('CMIP' and 'HTAP') employed distinct emission inventories with regard to anthropogenic emissions of aerosols and trace gases, yet utilized the grid resolution of the base case. Specifically, the CMIP6 model run utilized the CMIP6 database (O'Neill et al., 2016), while the HTAP model run employed the HTAPv3 database (Crippa et al., 2023).

An additional sensitivity model run was performed in which the thermodynamic state of the aerosol was altered ('THERM'). In this run, the metastable assumption was implemented, meaning aerosols are prevented from forming solids, even at extremely low RH values, allowing them to persist in a supersaturated aqueous phase. Additionally, a sensitivity model run was conducted in which the scavenging treatment was modified ('SCAV'), employing a simplified mechanism where the gas-to-particle phase partitioning follows the effective Henry's Law coefficients approach. Furthermore, no aqueous phase chemistry was considered in the calculation of cloud acidity, as a constant value of 5 was assumed for in-cloud and precipitation pH (Tost et al., 2007b). Another sensitivity model run ('HYDRO') concerns the treatment of the uptake of N₂O₅ hydrolysis, and more specifically the uptake coefficient considered. Specifically, an uptake coefficient for hydrolysis of 0.002 was employed (one order of magnitude lower than in the base case) in an attempt to obtain more accurate predictions in certain regions (Section 1).





Table 1: Configurations used in the base case and all sensitivity simulations.

Simulation Name	Spati	al Reso	lution		hropog missior			dynamic ate		enging tment	Ul	N ₂ O ₅ otake fficient
	T42	T63	T106	CAMS	CMIP6	HTAP	Stable	Metast.	Simple	Complex	0.02	0.002
Base Case		Х		Х			Х			Х	Х	
RES_low	Х			Х			Х			Х	Х	
RES_high			Х	Х			Х			Х	Х	
CMIP6		X			Х		Х			Х	Х	
НТАР		Х				Х	Х			Х	X	
THERM		Х		Х				Х		Х	Х	
SCAV		Х		Х			Х		Х		Х	
HYDRO		Х		Х			х			х		х

3. Evaluation of the Base Case Predictions for particulate NO₃

3.1 Surface concentrations and PM_{2.5} size fraction

The mean surface concentrations of $PM_{2.5}$ NO_3^- , and the size fraction of $PM_{2.5}$ NO_3^- (i.e., the fraction of $PM_{2.5}$ NO_3^- mass in respect to the total aerosol NO_3^- mass) are shown in Figure 1 for the entire period from 2010 to 2018. The maximum values of 14 μ g/m³ are predicted over the Indian subcontinent and the East Asian region, with Central Europe showing concentrations of ~5 μ g/m³ for the period average, while Turkey and Eastern USA show mostly concentrations of ~3 μ g/m³ (Fig. 1a). With respect to the size fraction, $PM_{2.5}$ accounts for more than 80% of the total particle concentration over the polluted northern hemisphere and up to 70% over South America, the southern part of Africa and Australia (Fig. 1b). The interaction of nitric acid with coarse mineral dust and sea salt particles results in smaller $PM_{2.5}$ size fractions. A 30% contribution is observed over the Southern Ocean, while the Arabian Peninsula region has the lowest predicted $NO_3^-PM_{2.5}$ fraction, with a value of less than 20%. Over the Western Sahara and the dust outflow directed towards South America, the $PM_{2.5}$ nitrate size fraction is around 60%.





313 314

315316317

318

319

320 321

322

323

324

325

326 327

328

329

330

331

332

333

334

335

336

337 338

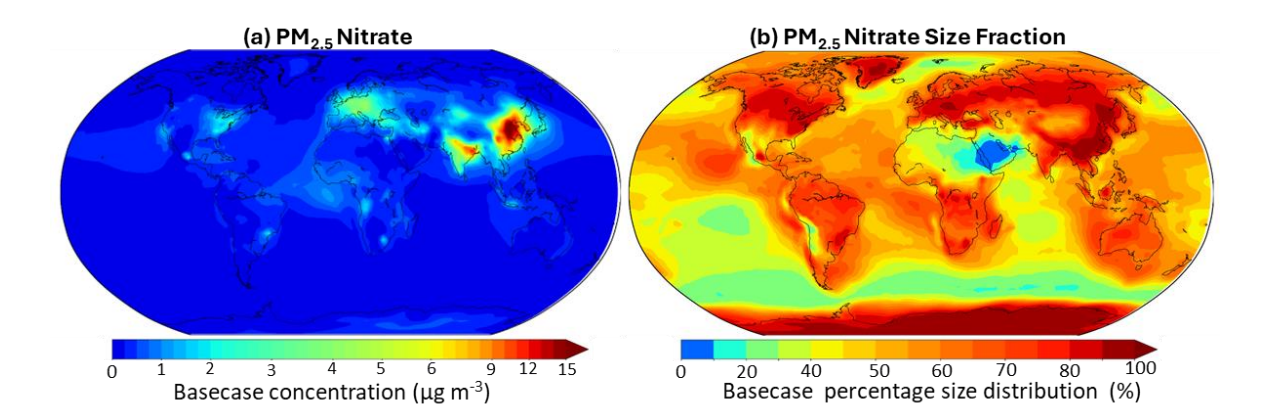
339

340

341

342

343 344



<u>Figure 1</u>: Annual mean (a) surface concentrations and (b) size fraction of $PM_{2.5}NO_3^-$ for the period 2010 - 2018 as simulated with EMAC from the base case.

3.2 Comparison of base case model results with PM_{2.5} observations

The PM_{2.5} aerosol observations are obtained from four networks that cover regions with the highest levels of anthropogenic activity in the polluted northern hemisphere. These networks include the EPA CASTNET network (U.S. Environmental Protection Agency Clean Air Status and Trends Network) and the IMPROVE network (Interagency Monitoring of Protected Visual Environments), which collectively encompass 152 stations for particulate nitrate across the United States. Notably, IMPROVE predominantly focuses on rural and remote regions, while EPA primarily covers urban areas. The EMEP network (European Monitoring and Evaluation Programme Air Pollutant Monitoring Data) includes nine stations for particulate nitrate, covering the European region. Additionally, the EANET network (The Acid Deposition Monitoring Network in East Asia) covers parts of East Asia with 33 stations. The locations of all stations can be found in Figure S1a. The above networks provide monthly measurements for the entire period under consideration in this study. Given the continuous nature of PM_{2.5} measurements, a comparison with model predictions is presented in the form of surface concentration maps, where the observations from each station are overlaid on the model concentration maps (see Figure 2). A comparison in the form of scatter plots of seasonal means can be found in Figure S2. The seasonal statistical evaluation for the comparison of PM_{2.5} nitrate is shown in Table 2. The metrics employed include Mean Absolute Gross Error (MAGE), Mean Bias (MB), Normalized Mean Error (NME), Normalized Mean Bias (NMB), and Root Mean Square Error (RMSE).

As illustrated in Figure 2a, the model can well reproduce the measurements with a high agreement for most stations in the USA, particularly those situated in the Midwestern region and along the Southern East Coast. However, discrepancies of approximately 1 μ g/m³ (model overprediction) are evident over the Central East stations, and discrepancies of approximately 2 μ g/m³ are observed for the larger areas of New York and Northern California. In Europe, the model's overprediction of low concentrations is evident in the Iberian Peninsula, the Baltic region, and Croatia (~3 μ g/m³ difference), while it more accurately represents the high concentrations observed in the UK and the Central and Western regions, with some exceptions in Germany and Switzerland (Fig. 3b). In East Asia, the discrepancy between model predictions and observations





is particularly pronounced. The model values for the North China Plain, Japan, Vietnam, and Thailand exceed the observed concentrations by up to $2 \mu g/m^3$, similar to the overprediction observed in Europe. However, the model values for Korea are three times higher than the observed concentrations (Fig. 3c). Conversely, the concentrations in the Zhangzhou region were underpredicted by the model, with discrepancies up to $5 \mu g/m^3$.

Statistically, the USA region demonstrates the most optimal model representation exhibiting differences to observations that are less than 1 μ g/m³ across all seasons. However, elevated normalized error values were observed during the summer and autumn periods. While the model shows higher overpredictions for East Asia, the mean bias and normalized error values appear to be relatively unaffected. However, the mean gross error and root mean square error metrics are notably larger compared to those observed for the USA. Notably, Europe exhibits the most significant discrepancies between model predictions and observations, with a mean bias exceeding 1 μ g/m³ and normalized error values particularly pronounced during the warm spring and summer periods, which are typically associated with low nitrate concentrations.

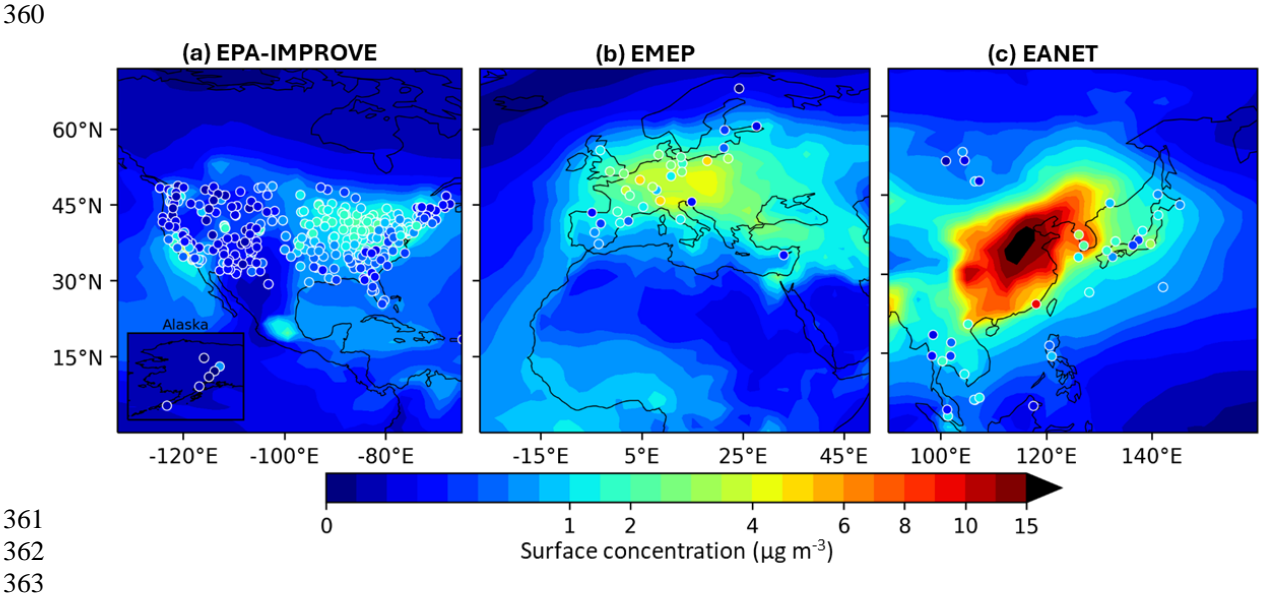


Figure 2: Average surface concentrations of $PM_{2.5} NO_3^-$ for the period 2010 - 2018 as simulated by EMAC from the base case (shaded contours) versus observations of the same species from the (a) EPA-IMPROVE, (b) EMEP and (c) EANET networks (colored circles).





Table 2: Seasonal statistical evaluation of EMAC simulated PM_{2.5} NO₃⁻ surface concentrations from the base case against observations during 2010-2018. The used metrics include the Mean Absolute Gross Error (MAGE), Mean Bias (MB), Normalized Mean Error (NME), Normalized Mean Bias (NMB) and Root Mean Square Error (RMSE).

		Number of	Mean Observed	Mean Predicted	MAGE	MB	NME	NMB	RMSE
Network	Season	datasets	$(\mu g m^{-3})$	$(\mu g m^{-3})$	$(\mu g m^{-3})$	$(\mu g m^{-3})$	(%)	(%)	$(\mu g m^{-3})$
EPA	Winter	144	2.8	2.4	1.4	-0.5	50	-16	2.2
	Spring	291	1.4	2.2	1.2	0.8	87	54	1.5
	Summer	280	0.5	0.8	0.5	0.3	103	59	0.9
	Autumn	290	0.7	0.9	0.6	0.2	89	37	0.9
IMPROVE	Winter	116	0.8	1.2	0.7	0.4	80	48	0.9
	Spring	233	0.5	1.1	0.7	0.6	131	112	0.9
	Summer	193	0.2	0.4	0.3	0.2	155	123	0.5
	Autumn	214	0.2	0.4	0.3	0.2	143	99	0.5
EMEP	Winter	7	3.4	3.9	2.5	0.6	74	16	3.3
	Spring	18	1.6	2.8	1.6	1.2	96	73	2.1
	Summer	18	0.3	1.5	1.3	1.2	461	451	1.8
	Autumn	17	0.8	2.7	1.9	1.9	241	233	2.8
EANET	Winter	30	2.0	2.5	1.6	0.4	80	21	2.6
	Spring	59	1.9	2.0	1.6	0.1	87	8	2.9
	Summer	59	0.6	1.6	1.4	0.9	217	147	2.6
	Autumn	59	0.8	0.8	0.7	0.0	85	3	1.1

3.3 Comparison of base case model results with PM₁ observations

The aerosol observations of PM_1 are derived from AMS measurements obtained during field campaigns in the Northern Hemisphere from 2010 to 2018. The measurement durations of these campaigns ranged from one to six months and included rural, urban, and downwind locations. The campaign and types of locations can be seen in Figure S1b. Further details regarding the locations of the field campaigns, including their duration, can be found in Tsimpidi et al. (2016; 2024). As the field observations (in contrast to the network measurements) are not continuous but rather fragmented into different time periods for each field campaign location, the comparison is presented in the form of scatter plots that compare the model and the measured values depending on the location type (see Figure 3). A scatter plot comparison of the seasonal means is shown in Figure S3. The statistical evaluation involves the regions of the USA, East Asia, Europe, and India, using the same metrics as above. The results are presented in Table 3.

As shown in Figure 3a, the model is able to reproduce the average PM_1 values over rural and urban locations in Europe with a high accuracy, although there is considerable variation at specific locations. On the other hand, it underpredicts PM_1 nitrate in urban downwind locations (up to





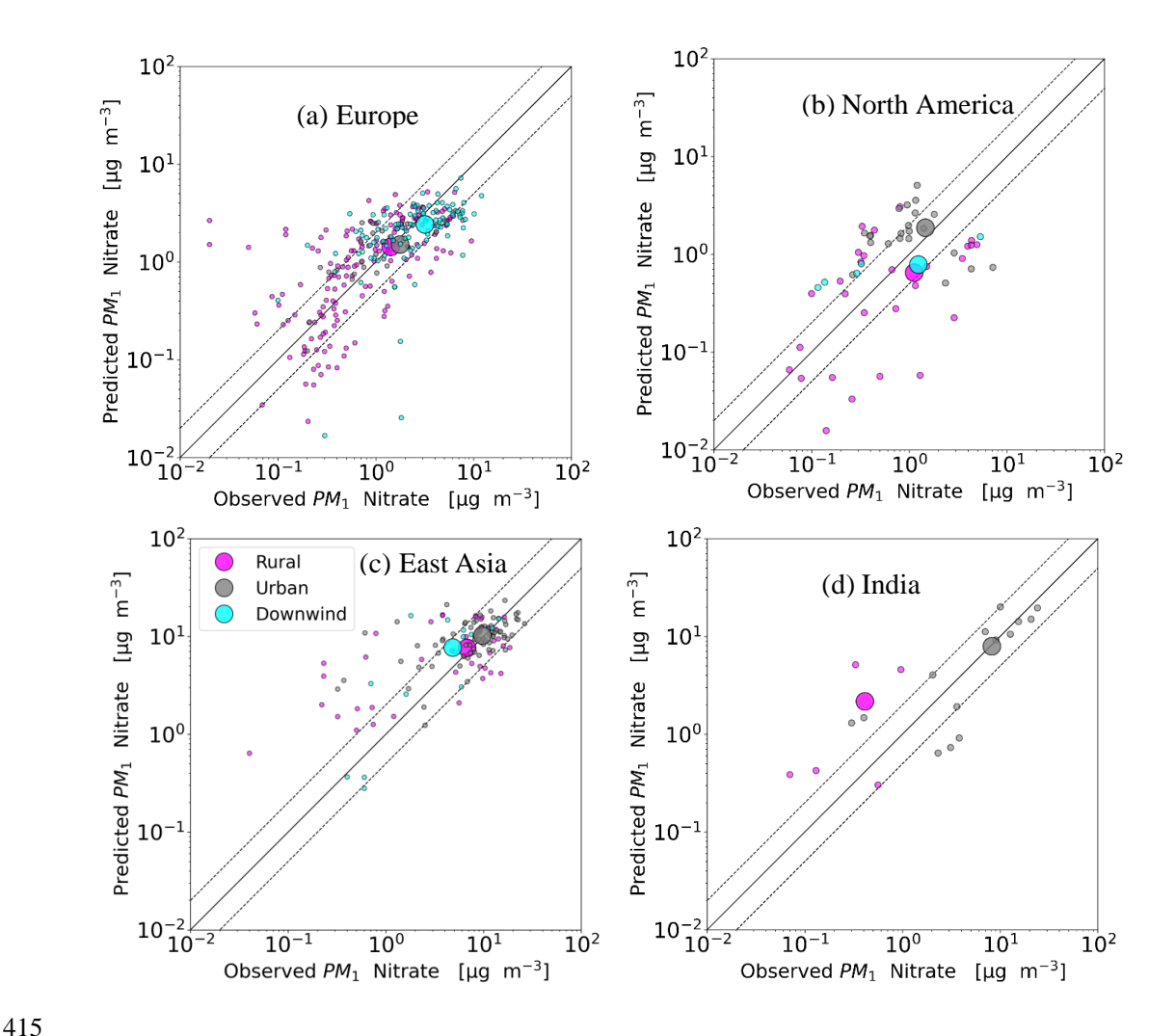
50%). In North America, the observed underprediction of average values is slightly stronger for downwind and particularly for rural locations (Fig. 3b) with average values for urban sites showing better agreement. In East Asia, the model shows similar accuracy to Europe in urban and rural locations, but with a significantly lower number of outliers (Fig. 3c). However, the average urban downwind values in this region exhibit an overprediction of slightly more than 50%. In India, the model's estimation of average urban values aligns closely with measurements, while the model significantly overestimates average rural values by a factor of 4 (Fig. 3d).

In contrast to the comparison of $PM_{2.5}$ concentrations, most of the metrics indicate that PM_1 aerosol observations in Europe are better reproduced. The USA shows low mean bias values and high scatter, as evidenced by normalized bias and error metrics. Conversely, East Asia shows higher absolute differences. The model has the worst performance for India, particularly in rural areas where there is a substantial discrepancy between the modeled and observed values. Overall, the model demonstrates a higher degree of accuracy in predicting PM_1 concentrations in both rural and urban locations as compared to downwind areas.

<u>Table 3</u>: Statistical evaluation of EMAC simulated PM₁ NO₃⁻ surface concentrations from the base case against observations during 2010-2018. The used metrics include the Mean Absolute Gross Error (MAGE), Mean Bias (MB), Normalized Mean Error (NME), Normalized Mean Bias (NMB) and Root Mean Square Error (RMSE).

		Number	Mean Observed	Mean Predicted	MAGE	MB	NME	NMB	RMSE
Region	Type of	of	$(\mu g m^{-3})$	$(\mu g m^{-3})$	$(\mu g m^{-3})$	$(\mu g m^{-3})$	(%)	(%)	$(\mu g m^{-3})$
	location	datasets							
USA	Rural	31	1.1	0.7	1.0	-0.5	88	-42	1.5
	Urban	22	1.5	1.8	1.6	0.4	111	25	2.1
	Downwind	5	1.2	0.8	1.1	-0.5	87	-36	1.7
East Asia	Rural	40	6.8	7.8	4.7	1.0	68	15	6.0
	Urban	78	9.7	10.3	4.0	0.6	41	6	5.2
	Downwind	15	4.9	7.9	3.5	3.0	71	61	5.2
Europe	Rural	163	1.4	1.4	0.9	0.0	62	1	1.4
	Urban	28	1.8	1.5	1.0	-0.2	54	-13	1.5
	Downwind	99	3.2	2.4	1.5	-0.7	48	-23	2.2
India	Rural	5	0.4	2.1	1.8	1.7	439	412	2.6
	Urban	14	8.2	7.8	4.0	-0.4	49	-5	5.2





<u>Figure 3</u>: Scatterplots comparing monthly mean surface concentrations of PM₁ NO₃⁻ as simulated by EMAC from the base case and measured by AMS instruments in field campaigns in the regions of (a) Europe, (b) North America, (c) East Asia and (d) India. Enlarged dots indicate the 2008 – 2018 period averages from all locations. Also shown are the 1:1 lines (solid) as well as the 2:1 and 1:2 lines (dashed).

4. Differences between PM_{2.5} and PM₁ NO₃⁻ concentrations in the sensitivity model runs

The differences in the predicted surface $PM_{2.5}$ nitrate concentrations across the sensitivity simulations in comparison to the base case, are illustrated in Figure 4. Furthermore, a comparison for $PM_{2.5}$ concentrations across different seasons can be seen in Figure 5 and a comparison of PM_1 concentrations for the different types of measurements sites in Figure 6, with detailed statistical metrics provided in Tables S1-S14.





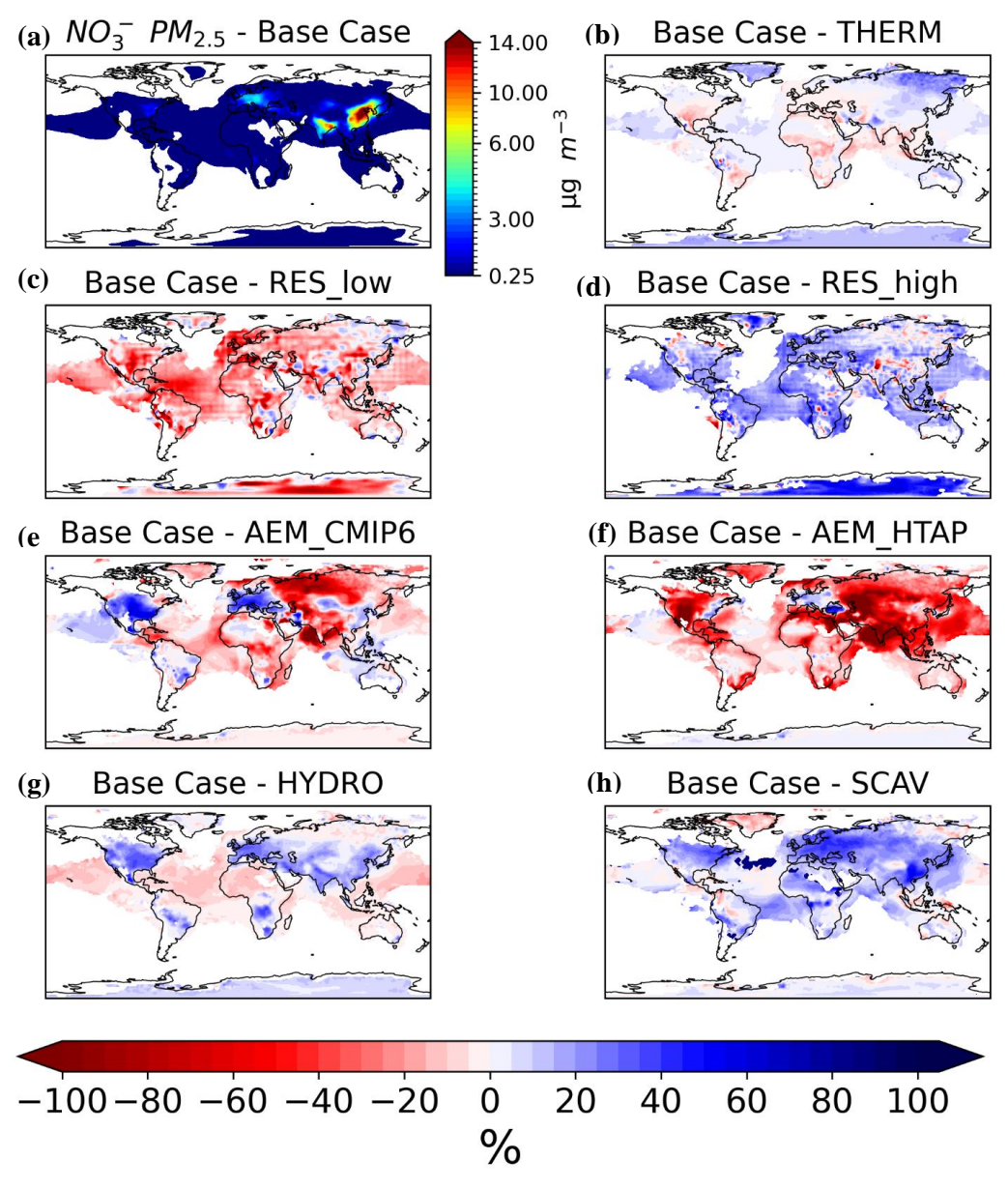


Figure 4: (a) Average surface concentrations of PM_{2.5} NO₃⁻ for the period of 2008 – 2018 as simulated by EMAC from the base case. White areas indicate average concentrations smaller than 0.25 μg/m³. Percentage changes of the EMAC-simulated average surface concentrations of PM_{2.5} NO₃⁻ between the base case model run and the (b) 'THERM' case (c) 'RES_low' case, (d) 'RES_high' case, (e) 'CMIP' case, (f) 'HTAP' case, (g) 'HYDRO' case and (h) 'SCAV' case model runs. Negative values in red indicate higher concentrations by the respective sensitivity case and positive values in blue indicate the opposite.





4.1 Sensitivity to the model spatial resolution

Lower Grid Resolution: Employing a coarser grid resolution generally predicts higher surface $PM_{2.5}$ nitrate concentrations than the base case (Fig. 4c). The largest differences (up to 80%) are observed for North America, followed by Europe (~30%). In East Asia, changes are more localized, with some areas exhibiting up to 15% lower values, while the Himalayan Plateau in India shows reductions of approximately 50%.

When evaluated against observational datasets, the lower-resolution sensitivity simulation closely reproduces mean winter and spring nitrate concentrations in Europe, where nitrate levels typically peak during these seasons (Fig. 5). However, the model significantly overestimates summer and autumn concentrations, with biases reaching factors of 3 to 4 for EMEP observations. In North America, this sensitivity case consistently overestimates nitrate levels, particularly during the warmer seasons, although winter concentrations are more in line with EPA observations. In contrast, the model overestimates PM_{2.5} nitrate levels observed in the IMPROVE network by up to three times, exhibiting comparable overestimations to those observed in EANET data. According to the statistical metrics, the lower-resolution model run does not outperform the base case, indicating that a coarser grid resolution does not increase the model's estimation accuracy.

For PM₁ nitrate concentrations, the lower-resolution case slightly overpredicts rural values in Europe by approximately 13%, while urban values are slightly underpredicted (Fig. 6). At downwind locations, the underprediction is more pronounced, reaching around 25%. In North America, this tendency is nearly reversed, with rural sites exhibiting a substantial underprediction (~30%) and urban sites showing an overprediction (~20%). Notably, downwind locations in this region are best represented by the lower-resolution sensitivity case. In East Asia, this case case shows very similar rural values to the base case, while urban sites display a moderate underprediction (~15%). However, at downwind locations, concentrations are significantly overpredicted, with nearly twice as high values as the observed values. In India, the lower grid resolution leads to the opposite behavior. In this case, concentrations in rural areas are overpredicted, similar to the base case results, while concentrations in urban areas show the largest underprediction among all sensitivity model runs, with concentrations being approximately a factor of 2.5 lower. Statistically, the lower-resolution case offers a slight improvement in accuracy for rural locations in North America and East Asia. However, it does not exceed the accuracy of the base case for Europe or India.

Higher Grid Resolution: In contrast to the results of the low grid resolution, simulations employing a higher grid resolution have yielded reduced surface $PM_{2.5}$ nitrate concentrations in comparison to the base case (Fig. 4d). The differences in nitrate concentrations can reach up to 50% across North America, Europe, and India, with less consistent patterns in East Asia.

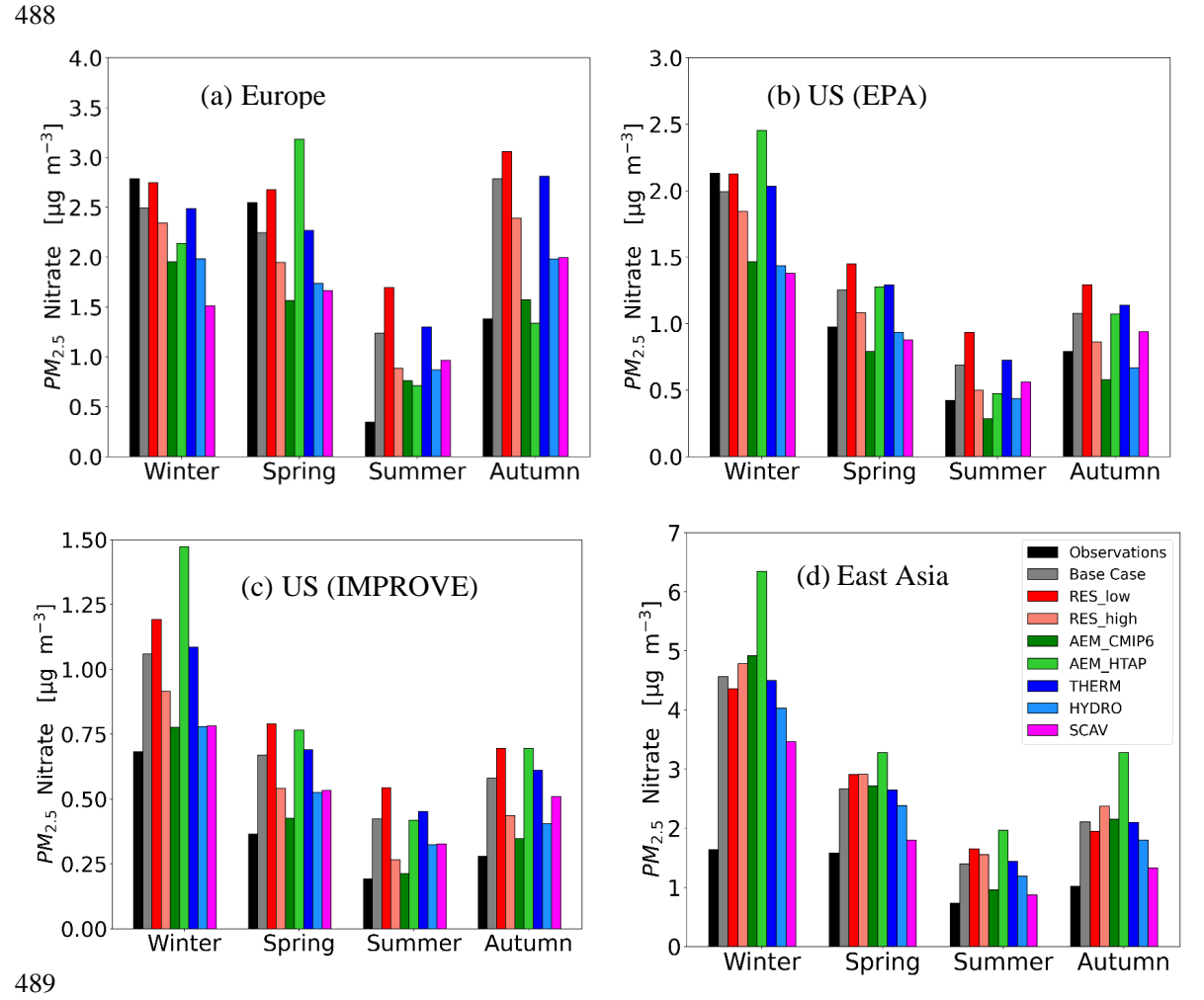
A comparison of the high-resolution model run with the EMEP observations reveals that it underpredicts nitrate concentrations in winter and spring by approximately 20%, but performs better in summer and autumn, reducing the overestimation compared to the base case (Fig. 5). Similarly, the higher grid resolution provides more accurate predictions for EPA observations in most seasons except winter, when slight underestimations occur. For the IMPROVE network, the high-resolution case achieves the best agreement in summer, though its performance varies across other seasons.

For PM₁ nitrate, the high grid resolution provides a modest underprediction across all European location types, with the most substantial discrepancy observed at downwind sites (\sim 33%). In North America, rural and downwind sites exhibit a more pronounced underprediction, reaching up to a factor of 2, while urban locations show a modest overprediction (\sim 12%). In contrast, the results





for East Asia exhibit an opposing pattern, with observations from all location types slightly overpredicted by the model, particularly at downwind sites (~factor of 2). In India, the urban locations estimate by this sensitivity align closely with the base case results, while rural sites demonstrate a marginally higher overprediction. Statistically, the high grid resolution enhances the accuracy of model predictions for urban sites in North America and Europe while also improving rural predictions in East Asia, underscoring its effectiveness in capturing finer spatial variability.



<u>Figure 5</u>: Average seasonal surface concentrations of PM_{2.5} NO₃⁻ measured (black bars) and predicted from the base case and all sensitivity cases (colored bars) for the networks of (a) EMEP, (b) EPA, (c) IMPROVE and (d) EANET during winter, spring, summer and autumn.





4.2 Sensitivity to anthropogenic emission inventories

CMIP6: The application of the CMIP6 anthropogenic emission inventory for the simulation of surface PM_{2.5} nitrate concentrations provides lower concentrations in most regions, except for India (Fig. 4e). The most significant reductions in surface PM_{2.5} nitrate concentrations are observed in North America and Europe (50%-60%). East Asia exhibits a comparatively smaller reduction, ranging from 10% to 20%. Conversely, India exhibits an increase in PM_{2.5} nitrate levels ranging from 30% to 40%.

A comparison with observations reveals notable discrepancies (Fig. 5). For EMEP observations, the CMIP emission inventory underestimates winter and spring concentrations by up to 40%, while overestimating summer values (by twofold), although autumn values are well captured. For EPA observations, this case underestimates in all seasons except winter, yielding the lowest PM_{2.5} nitrate predictions among all cases. Interestingly, the underestimation during most seasons is analogous to the overestimation seen in the 'RES_high' case. For IMPROVE observations, model predictions are more accurate, characterized by minor positive biases (less than 10%), with summer values showing enhancement over the base case. For EANET observations, summer values are improved compared to the base case model, but values are overpredicted for other seasons similar to the base case model results. Statistically, the 'CMIP' case demonstrates greater efficacy than the base case for most observational networks, with the exception of EANET, for which similar results are obtained.

A comparison of the 'CMIP' model run with observations of PM₁ nitrate concentrations measured by AMS instruments in field campaigns reveals the largest underprediction of all sensitivity model runs for all location types in Europe, with downwind sites showing the largest discrepancy (~factor of 2). A similar pattern is observed in North America, where rural sites show differences as high as 80%. In contrast, observations in East Asia are more closely aligned with this case. Values in rural sites show the best agreement with observations, while values in urban sites exhibit only a slight underprediction of less than 10%. In downwind locations, however, values are moderately overpredicted by approximately 25%. In India, the CMIP emission inventory results in an overprediction of observations of around 20% in urban areas, with values in rural areas showing an even greater discrepancy, reaching approximately a factor of 10. Statistically, this case performs worse than the base case for Europe and India, however, has an improved performance in East Asia and the USA, particularly for metrics other than MB and NMB.

HTAP: The simulation using the HTAPv3 anthropogenic emission inventory generally predicts higher $PM_{2.5}$ nitrate concentrations than the base case (Fig. 4f). Notably, Europe and the eastern United States constitute exceptions, exhibiting 20–30% lower concentrations compared to the base case model. In other regions, particularly western North America and India, the predicted concentrations are up to 100% higher than in the base case model, with values in East Asia showing increases of 60–80%.

A comparison of the model results with observations reveals significant variations. For EMEP observations, the HTAP emission inventory underestimates values in winter, similar to the 'CMIP' case, and overestimates concentrations in summer. Notably, the 'HTAP' model run exhibits the most significant underestimation in spring, reaching approximately 60%. However, the model's performance is satisfactory in the autumn. Comparisons to EPA observations show a consistent overestimation in all seasons, opposite to results of the CMIP6 model run. Comparison of the HTAP model results to the IMPROVE data show an overestimation of values (~factor of 2), particularly in winter, similar to results of the RES_low model run. For EANET observations, the use of the HTAP emission inventory leads to high overpredictions, ranging from a factor of 2 in

https://doi.org/10.5194/egusphere-2025-313 Preprint. Discussion started: 12 February 2025 © Author(s) 2025. CC BY 4.0 License.



541

542

543

544

545

546

547

548

549

550

551

552

553554

555

556

557

558

559

560

561 562

563

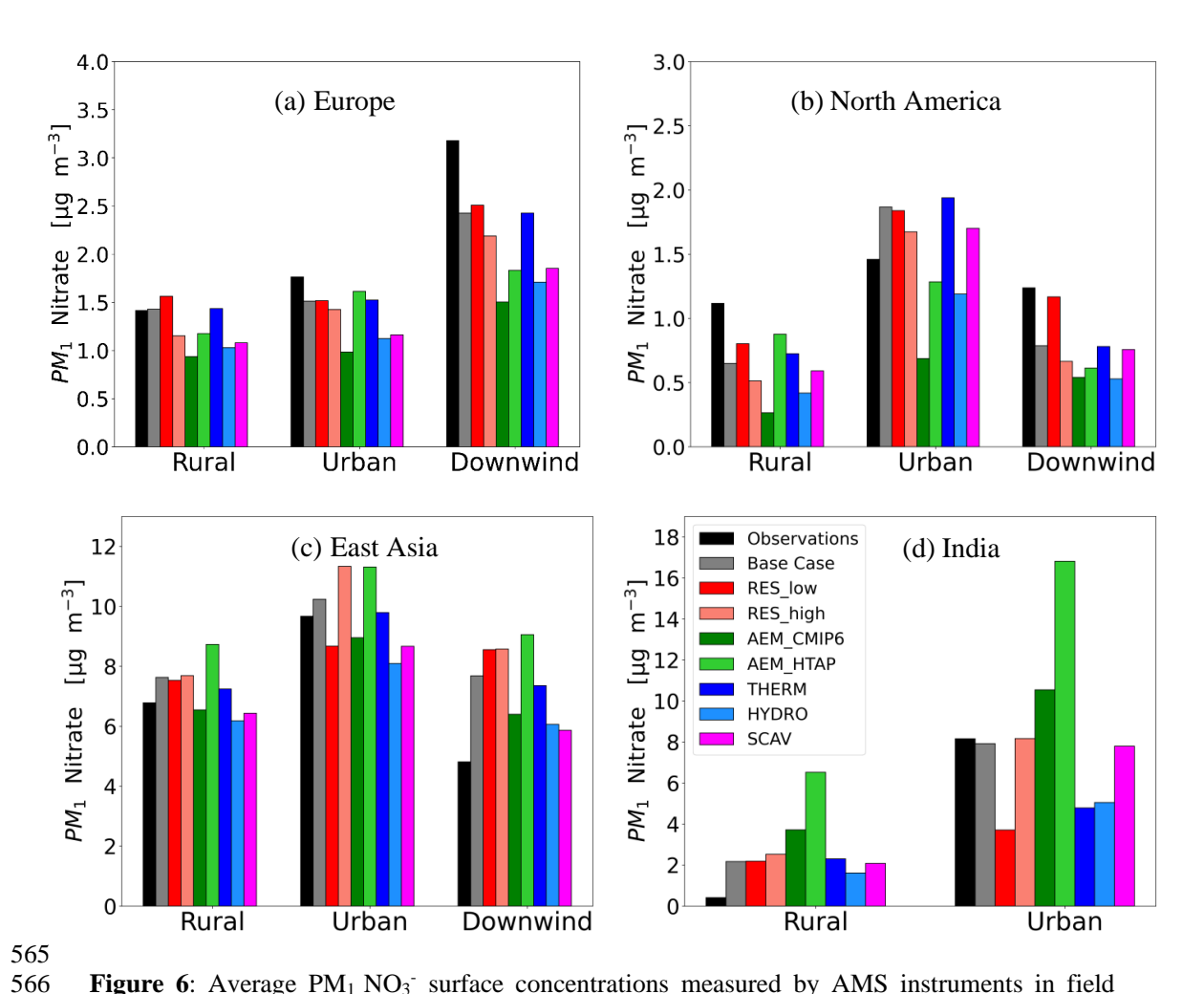
564



spring and summer to a factor of 4 in winter. Statistically, the HTAP model run performs better than the base case model for EMEP observations during summer and autumn, but model predictions are worse in winter and spring. Slight improvements are observed for EPA observations, while the model performance is worse for IMPROVE observations, and especially for EANET observations.

When evaluated against PM₁ nitrate concentrations measured by AMS instruments in field campaigns, the HTAP emission inventory shows a 20% underprediction of values at rural sites in Europe, but it best captured average urban values compared to all other sensitivity simulations. However, in downwind locations, the model underpredicts concentrations by nearly 40%. This sensitivity model run performs particularly well compared to observations in North America, where it shows the best agreement with observations in both rural and urban locations. However, in downwind locations, the model values are significantly lower than the observations, similar to the base case estimates, with a model-measurement discrepancy of nearly 50%. In contrast, reproducing observations in East Asia appears to be challenging for this sensitivity case, as the simulated values show the highest overprediction of all model cases for all location types. The results for downwind sites exhibit a distinct overprediction of almost a factor of 2, while results for other locations show discrepancies of less than 20%. In India, concentrations simulated by the 'HTAP' case show a substantial overprediction for both urban and rural locations, and the most significant model-measurement discrepancies among all sensitivity model runs. In rural areas, the overprediction can reach up to a factor of 15, while in urban areas, the predicted concentrations are approximately double the observed values. Statistically, the 'HTAP' case performs worse relative to the base case in East Asia and India. However, it provides improved predictions for rural locations in the USA and Europe, but not for urban downwind sites.





<u>Figure 6</u>: Average PM₁ NO₃⁻ surface concentrations measured by AMS instruments in field campaigns (black bars) and predicted by the base case and all sensitivity cases (colored bars) for the regions of (a) Europe, (b) North America, (c) East Asia and (d) India divided into rural, urban and downwind locations.

4.3 Sensitivity to the model treatment of the aerosol thermodynamic state and chemistry

Metastable state: The simulation assuming a metastable thermodynamic state (aerosols do not precipitate into solid salts at low humidity) indicates only minor discrepancies in surface $PM_{2.5}$ nitrate concentrations compared to the base case (Fig. 4b). Concentrations exhibit a 10-15% increase in North America and Europe, while in the Himalayan Plateau, they decrease by up to 30%, and in East Asia, they are slightly lower.

When evaluated against $PM_{2.5}$ observations, the metastable state performs almost identically to the stable state (i.e., base case) for all observational networks. However, slightly less accurate





predictions (differences <5%) are observed for the EPA and IMPROVE networks, as reflected in the statistically insignificant differences between the metrics derived for the sensitivity and base case model runs.

For observations of PM_1 nitrate concentrations, the metastable results are nearly identical to the base case model run in Europe and North America for all location types. A similar behavior is observed in East Asia, where the metastable assumption overpredicts observed concentrations by approximately 5% compared to the base case model run for all locations. In India, the metastable and base case results show no difference in rural areas, but values are underpredicted by about 40% in urban areas due to the use of the metastable state assumption. This discrepancy is associated with the combination of moderate temperatures and low relative humidity at these locations, which hinder the partitioning of nitrate into the aerosol phase (Ansari and Pandis, 2000; Milousis et al., 2024). These factors contribute to the model-measurement discrepancies, particularly in urban areas with elevated nitrate aerosol concentrations. Statistically, this particular sensitivity performs marginally better than the base case model run for downwind sites in East Asia. However, it underestimates nitrate concentrations at urban sites in India, with only minor discrepancies to observed values elsewhere.

Lower N_2O_5 uptake coefficient for hydrolysis: The simulation that incorporated a lower uptake coefficient for N_2O_5 hydrolysis consistently yielded lower surface $PM_{2.5}$ nitrate concentrations in all regions when compared to the base case model (Fig. 5g). The simulation indicates a 20% decrease in East Asia and a 40% decrease in Europe and North America, reflecting the suppression of nitrate formation via the hydrolysis pathway.

A comparison of the model simulation using a lower N₂O₅ uptake coefficient with observations reveals a tendency to underpredict the PM_{2.5} nitrate concentrations from the EMEP network during winter and spring. The discrepancy between this simulation case and the observations is more pronounced in winter and spring (25% and 35%, respectively) compared to summer and autumn. For the EPA network, this sensitivity underpredicts winter values by approximately 30%, but gives better agreement for all other seasons than any of the other sensitivity cases. Against IMPROVE observations, the lower N₂O₅ uptake coefficient case results in a lower overprediction in all seasons when compared to the base case model run. The model-measurement differences are within 30%. For EANET observations, the HYDRO model simulation gives values that are in better agreement with the observations than the results of the other sensitivity model runs, exception for the 'CMIP' case during summer. Statistically, the 'HYDRO' case shows improved performance compared to the base case across all observational networks and metrics, with the exception of the EANET observations during the autumn season. The most significant improvements compared to the base case are observed for the EPA network, as this scenario showed the best metrics in comparison to the rest of the sensitivities, for values obtained in summer and autumn.

For PM_1 nitrate concentrations, the sensitivity case with lower N_2O_5 uptake exhibits the second highest underprediction among all sensitivity model runs, surpassed only by the 'CMIP' case, across all location types in Europe. A similar behavior was observed for North American values. However, the results of the model-measurement comparison vary significantly for values in East Asia. Specifically, while the 'HYDRO' model run demonstrates the most significant underprediction for urban site values (approximately 15%) among all other sensitivity cases, it exhibits a lower overprediction bias compared to the base case for both rural and downwind locations, resulting in a closer agreement with the measurements. In India, the HYDRO case exhibits the lowest overprediction for rural values among all sensitivity model runs, although these values are substantially lower (a factor of 4) than the observations. For urban areas, the lower N_2O_5





uptake coefficient results in an underprediction comparable to that obtained by using a lower grid resolution or by assuming a metastable aerosol state. Statistically, the 'HYDRO' case demonstrates a lower performance than the base case in Europe, particularly for rural and downwind locations, as evidenced by the presence of stronger negative biases and higher error rates. In North America, the model performs worse for rural locations but better for urban locations, with comparable metrics for urban downwind predictions. In East Asia, the lower N₂O₅ uptake coefficient provides more accurate predictions than the base case for rural and downwind locations for most metrics (except for RMSE), yet predictions are less precise for urban sites. In India, the predictions in rural areas are improved compared to the base case model run by this sensitivity, but predictions in urban areas remain unchanged. This observation indicates that the 'HYDRO' model run performs better in capturing nighttime aerosol nitrate formation, which is predominant in rural areas. In contrast, daytime production pathways seem to be more significant in urban areas.

4.4 Sensitivity to the scavenging treatment

Simplified scavenging treatment: The implementation of a simplified scavenging treatment for the gas phase aerosol precursors in the model (Section 2.3) yields substantially reduced surface PM_{2.5} nitrate concentrations compared to the base case (Fig. 4h). The largest differences are found for Europe and East Asia, where concentrations are reduced by approximately 60%. Comparatively, North America exhibits a reduction of approximately 30%, while India experiences a decline of around 10–20%. These lower concentrations can be attributed to the high wet deposition fluxes in the simplified mechanism, which neglects gas-phase diffusion limitations and assumes an equilibrium between the gas and aerosol phases (Tost et al., 2007b). Additionally, the assumed pH of 5 for clouds and precipitation is less acidic than typical for polluted regions, further enhancing nitrate scavenging.

A comparison of the 'SCAV' case with observations reveals the strongest underprediction for EMEP measurements in winter (~45%). Overprediction biases are less by ~20% and ~30%, respectively, than in the base case model run during summer and autumn. For the EPA network, the 'SCAV' case demonstrates the most significant overprediction of observations in winter (~45%) among all sensitivity model runs. However, values are only marginally overpredicted in the other seasons (~10%), and even slightly underpredicted in spring. The simplified scavenging treatment better reproduces the IMPROVE observations throughout the year compared to the base case, with notable reductions in model-measurement discrepancies of up to ~40% during winter and spring. For EANET observations, the 'SCAV' model run yielded smaller values than the base case, thereby reducing the overprediction bias by ~35% during winter. In all other seasons within the region, this particular sensitivity demonstrates the smallest discrepancies between model predictions and observations among the rest. Statistically, the 'SCAV' case demonstrates enhanced performance in comparison to the base case for EMEP and EPA observations across the majority of seasons, with the exception of winter, where the model exhibits a substantial underprediction tendency, as evidenced by both bias and error metrics. The model-measurement agreement for observations of the IMPROVE network exhibited enhancement in comparison to the base case model run across all seasons. The agreement for EANET observations shows improvements only during winter and summer, while during spring and autumn the statistical metrics of the 'SCAV' case are worse compared to the base case.

For PM₁ nitrate, the simplified scavenging treatment underpredicts the observations more than the base case for all location types in Europe. The magnitude of the bias observed in the 'SCAV' case is comparable to that obtained by using the CMIP6 emission inventory or by using a lower





N₂O₅ uptake coefficient. In North America, the simplified scavenging treatment results in an underprediction of concentrations of approximately 50% for rural sites and 40% for downwind sites, though it is slightly smaller than the overprediction bias of the base case model for urban locations. In East Asia, the 'SCAV' case exhibits a smaller overprediction of observed values compared to the base case results for downwind locations (~25%), while this sensitivity provides nearly identical estimates for rural sites. Conversely, urban sites exhibit a slight underprediction (12%) in this sensitivity analysis. In India, the 'SCAV' sensitivity model run does not lead to substantial changes in the estimates compared to the base case results for both urban and rural locations. Statistically, the 'SCAV' case performs worse than the base case in terms of bias metrics for results in Europe, although the discrepancy in error metrics is less pronounced. In North America, the 'SCAV' case shows worse metrics for rural sites, but shows improvements for urban sites. Downwind sites show increased biases but reduced errors. In East Asia, the 'SCAV' case exhibits higher accuracy in capturing observations at rural and downwind sites compared to the base case but performs less successfully at urban sites. A similar pattern is observed in the results for India. In summary, when evaluated against the metrics of the base case, the 'SCAV' case yielded enhancements for rural sites in Europe and India.

5. Temporal Variability and Tropospheric Burden of NO₃

The availability of continuous time series data from monitoring networks for $PM_{2.5}$ nitrate concentrations facilitates a comparison of seasonal patterns across different model sensitivities and regions. Conversely, the PM_1 measurements, which were campaign-based and characterized by varying durations, lack the capability to facilitate a comparable seasonal analysis. Consequently, a selection of stations measuring PM_1 nitrate concentrations in Europe was chosen, as the model in this region had difficulty in reproducing observed concentrations for this size mode. These stations, which provide hourly measurements, facilitate a detailed comparison of the diurnal variation of modeled and observed data. Finally, this section includes an analysis of the total tropospheric burden of nitrate aerosols. This analysis compares estimates from all sensitivity cases to assess their global-scale implications. This multi-scale approach aims to highlight the temporal dynamics and atmospheric significance of nitrate aerosols in relation to different modeling configurations.

5.1 Seasonal variation of PM_{2.5} concentrations

Figure 7 presents the seasonal patterns of PM_{2.5} predictions from model sensitivity runs and measurements obtained from observational networks in the specified regions. For the EMEP network, all sensitivity simulations consistently underpredicted the PM_{2.5} concentrations from January to April, with the largest discrepancies observed in March, ranging from 35% for the lower grid resolution case to 55% for the case using a simplified scavenging treatment. It is noteworthy that the 'HTAP' case is the only model run that accurately reproduces this period, including the peak concentration observed in the measurements in March. Conversely, from April to December, the majority of sensitivity cases exhibit an overprediction of observed concentrations, with the exception of the 'HTAP' case after October. The most pronounced overestimations are observed in the run with the lower spatial resolution and the base case, with concentrations reaching up to twice the observed levels in October. In contrast, the 'CMIP' and 'HYDRO' cases exhibit smaller discrepancies between model and measurement, with model overestimations of approximately 40%. While all model cases captured the general seasonal cycle, the 'HTAP' case did not capture the exact timing of the second maximum, which was shifted one month earlier and showed a



717

718

719

720

721

722

723

724 725

726

727

728

729

730

731

732

733

734

735

736 737

738

739

740

741

742

743

744

745

746

747

748

749

750

751

752

753

754

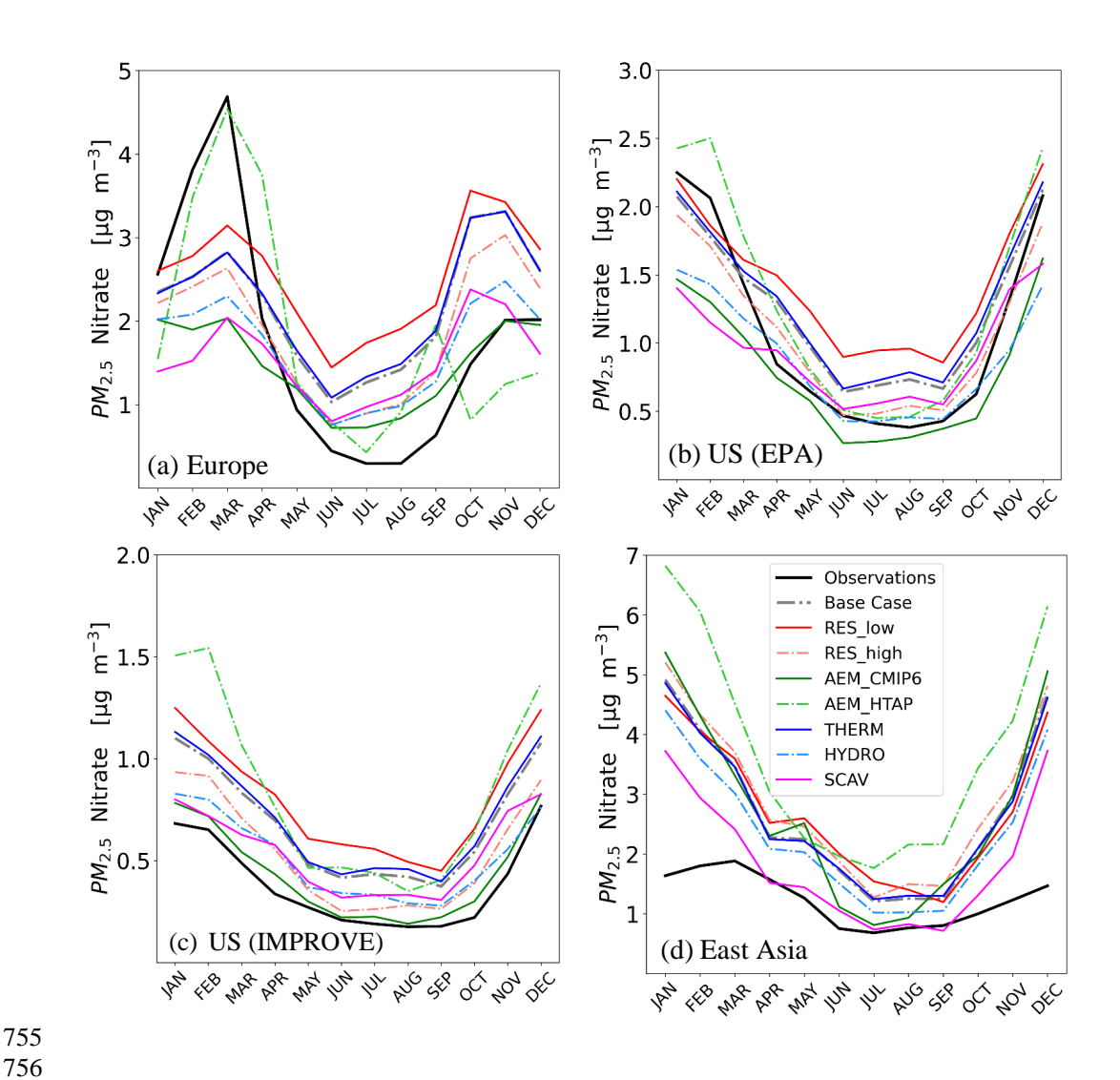


stronger post-summer decline compared to the other model runs. The results of the 'CMIP' case, followed by the 'RES_high' and 'HYDRO' cases, give the closest agreement with observations, particularly at low nitrate concentrations. Overall, the magnitude of model overpredictions is most pronounced during summer and early autumn. The enhanced discrepancies between model projections and observations for this network can be partially attributed to the increased evaporation of the semi-volatile nitrate aerosol species under warm conditions (Ames and Malm, 2001; Docherty et al., 2011) from the nylon filters used by the EMEP samplers (Yu et al., 2005).

A similar seasonal pattern is observed in the USA when comparing model outputs to EPA measurements, with underpredictions of observed values from January to April and overpredictions from April to December. The 'SCAV' case demonstrates the most significant underprediction of observations, exhibiting a 35% discrepancy in February. In contrast, the lowerresolution case reveals the most substantial overprediction, with concentrations surpassing observations by a factor of 2 in August. The sensitivity model runs with different anthropogenic emission inventories demonstrate contrasting behaviors, with the HTAPv3 consistently overpredicting the measured concentrations and the CMIP6 underpredicting them. Despite these biases, the seasonal variation is adequately captured in all model cases, with the high-resolution and the metastable model runs demonstrating the most optimal overall performance. A similar pattern to the European region was observed, where the warm months were also characterized by the largest overprediction biases of the year for this network. This phenomenon is attributed, at least in part, to biases associated with evaporation losses from the filter samplers during this particular season. Under warmer weather conditions, increased filter temperatures lead to increased evaporation of semi-volatile species such as nitrate (Ames and Malm, 2001; Docherty et al., 2011). For the IMPROVE network, all model cases exhibit overpredictions of PM_{2.5} concentrations throughout the year, with more pronounced discrepancies observed during colder months. During these months, the HTAP emission scenario shows differences up to a factor of 2.5 in February and a factor of 2 in December, while the low-resolution scenario shows comparable deviations in spring and summer. Among the sensitivity cases, the model run with the CMIP6 emission inventory shows the best agreement with the observations, followed by the 'SCAV' case during the early months of the year and the high-resolution and metastable sensitivities during the remainder of the year.

The EANET network shows a similar seasonal variability to the IMPROVE network, with all model cases consistently predicting higher concentrations than observed throughout the year, while successfully reproducing the observed seasonality. The most pronounced overpredictions occur during the cold months, with the HTAP emission inventory exhibiting the most significant deviations of up to a factor of 3.5 in January. The 'SCAV' case demonstrates the most favorable agreement with observations, exhibiting deviations that remain constrained to a factor of 1.5 during the cold season. This suggests that the intricate aerosol scavenging process included in the base case may potentially underestimate the wet deposition fluxes of particulate nitrate in this region. The HYDRO and CMIP6 cases also perform well, particularly for lower concentrations.





<u>Figure 7:</u> Seasonal variation of measured (black lines) and predicted (colored lines) PM_{2.5} NO₃ surface concentrations from the base case and all sensitivity model cases for the networks of (a) EMEP, (b) EPA, (c) IMPROVE and (d) EANET.

5.2 Diurnal variation of PM₁ concentrations

Figure 8 presents a comparison of the diurnal variation of the simulated PM_1 nitrate concentrations from the base case and sensitivity model runs against hourly observations from seven European stations. At Birkenes, most simulation cases can capture the observed diurnal pattern, with concentrations peaking in the early morning and decreasing in the late evening. However, the low-resolution case deviates significantly, with concentrations that are twice the observed values. The high-resolution case results are closest to the observations, suggesting that a





higher grid resolution is more effective in capturing the variations in aerosol nitrate concentrations induced by anthropogenic activities during the day. Conversely, the 'SCAV' model run exhibited the most significant underprediction, reaching a factor of 2. In Bucharest, the model sensitivities yielded a comparable morning peak, albeit smaller than the observed value, occurring approximately two hours earlier than the observed peak. Although an evening minimum of PM₁ nitrate is predicted at a similar time, the model significantly underpredicts afternoon concentrations, with the discrepancy being twice as large as that for the morning values. The simulation with the high-resolution had the best performance compared to the other cases for this station, which has a diurnal pattern similar to the previous station, followed by the base and metastable state assumption. The 'SCAV' case demonstrates the most significant diurnal variability among the rest of the sensitivities, exhibiting a pronounced decrease in concentrations during the transition from day to night.

At Hohenpeissenberg, the model results fail to reproduce the observed early morning minimum. Predicted late morning maxima and afternoon minima are higher than the observations in most cases, except for the high-resolution, metastable, and CMIP6 cases. During the early morning hours, these three cases demonstrate the smallest discrepancies with the observations, while the low-resolution exhibits a stronger agreement in the afternoon due to a less pronounced decline in the modeled concentrations. The elevation of the station, 300 meters above the surrounding area, serves to reduce the influence of anthropogenically influenced air masses, thereby reducing the variability observed in the hourly values. However, this is not reflected in the model results.

At Melpitz, the observed diurnal pattern is well reproduced by the model results. In most sensitivity cases, morning values are marginally higher than observed values, while evening values are slightly lower. The CMIP6 emissions demonstrate the most accurate morning values among the diverse model runs, while the base and metastable exhibit more precise evening concentration predictions compared to the others. The lower-resolution run demonstrates the most overall agreement with observations throughout the day, attributable to the less pronounced maximum and minimum peaks.

For the SIRTA station, the model results adequately capture the diurnal pattern, though the evening minimum values are predicted three hours later than observed. The lower- and higher-resolution cases demonstrated an enhanced representation of the morning maximum compared to the other cases, while the lower spatial resolution exhibited superior prediction of the evening minimum compared to all other sensitivities. This case also demonstrated a less pronounced transition from daytime to nighttime values, similar to the previous comparison. The other model sensitivity cases underpredict the observations, with discrepancies ranging from 40% ('HTAP' case) to a factor of 3 ('CMIP' case).

At Puy De Dôme, the model results fail to reproduce the diurnal variation of the observations. As this station is located on one of the highest peaks of the Chaîne des Puy, the station is representative of the regional atmospheric conditions. This characteristic is evidenced by the absence of a pronounced diurnal variation in PM₁ levels, in contrast to what is observed in more polluted locations such as Bucharest and SIRTA. The morning values are marginally overpredicted by the lower spatial resolution; however, evening values are consistently underpredicted by all sensitivities, at a time when the observations showed nearly constant values. The lower-resolution run exhibits the least deviation from observations in the afternoon, while the base and metastable state demonstrate more accurate performance in the early morning.

At Villeneuve, the observed diurnal pattern is generally well reproduced by the model results, except for a three-to-four-hour delay in the observed evening minimum. It is evident that all cases

https://doi.org/10.5194/egusphere-2025-313 Preprint. Discussion started: 12 February 2025 © Author(s) 2025. CC BY 4.0 License.





exhibit an underprediction of the observed concentrations, with the most pronounced discrepancies observed in the sensitivity case using the HTAPv3 emissions, reaching up to a factor of 3, and the least significant discrepancies observed in the base case and the metastable, at approximately 60%.

The analysis indicates that the grid resolution is the most critical factor in reproducing the diurnal variability of PM_1 nitrate concentrations. For stations exhibiting regional characteristics (Hohenpeissenberg, Melpitz, and Puy De Dôme), the lower spatial resolution provides optimal predictions during the day, while it more accurately captures evening and nighttime values. The observed discrepancy during nighttime hours can be attributed to the distortion of NO_x fields resulting from the larger grid cells. This distortion leads to elevated nitrate radical concentrations and increased nitrate aerosol production during nighttime hours, a process that has the greatest impact on rural areas (Zakoura and Pandis, 2018). Consequently, the low-resolution case results in increased nighttime concentrations that approximate the observed values. The base case and metastable state assumption demonstrate satisfactory performance across all stations, while the use of a lower N_2O_5 uptake coefficient provides minimal improvement compared to the base case. For the sensitivity model runs employing different emission inventories, the HTAPv3 outperforms the CMIP6; however, the agreement between modeled values and observations remains less than that for the base case. This outcome confirms the suitability of the CAMS database for modeling European PM_1 nitrate concentrations.



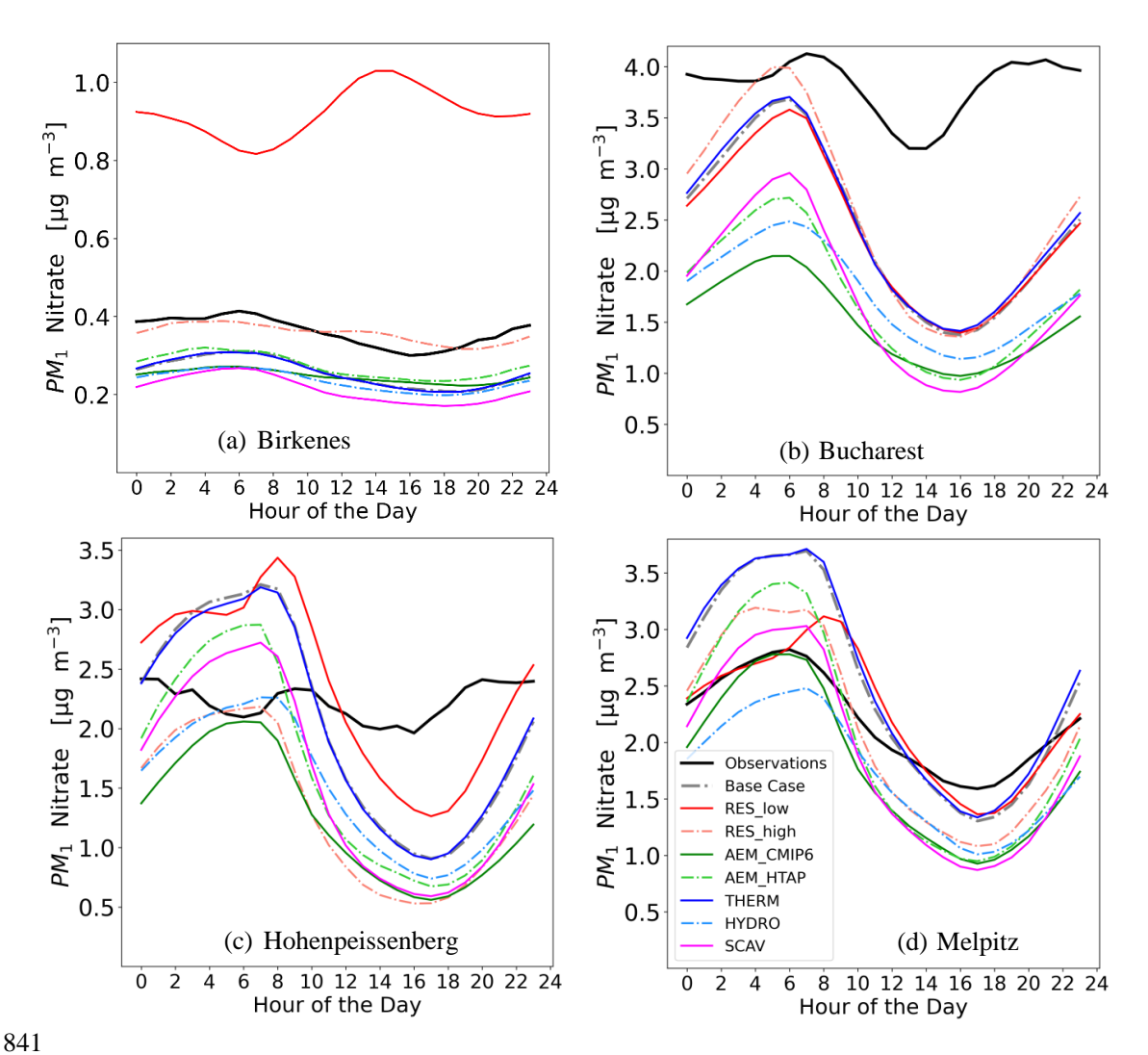


<u>Table 4</u>: Names, locations and data availability of the stations used for the comparison of diurnal $PM_1 NO_3^-$ concentrations. The location type of each station is also categorized as rural (RUR) or downwind (DW) locations.

Station Name	Station Code	Longitude	Latitude	Availability of hourly data
Birkenes II (RUR)	NO0002R	58°23'19"N	008°15'07"E	8/2012 - 8/2018
Bucharest (DW)	RO0007R	44.344°N	26.012°E	8/2016 - 8/2018
Hohenpeissenberg (DW)	DE0043G	47°48'05"N	011°00'35"E	4/2015 - 10/2015 1/2017 - 9/2017 10/2017 - 11/2018
Melpitz (RUR)	DE0044R	51°31'49"N	012°56′02"E	7/2015 – 9/2015 5/2016 – 11/2017
Puy de Dôme (RUR)	FR0030R	45°46'00"N	002°57'00"E	3/2015 - 10/2016 1/2018 - 12/2018
SIRTA Atmospheric Research Observatory (DW)	FR0020R	48°42'31"N	002°09'32"E	10/2014 – 1/2016
Villeneuve d'Ascq (DW)	FR0027U	50.611°N	3.14°E	10/2016 – 11/2017 7/2018 – 12/2018



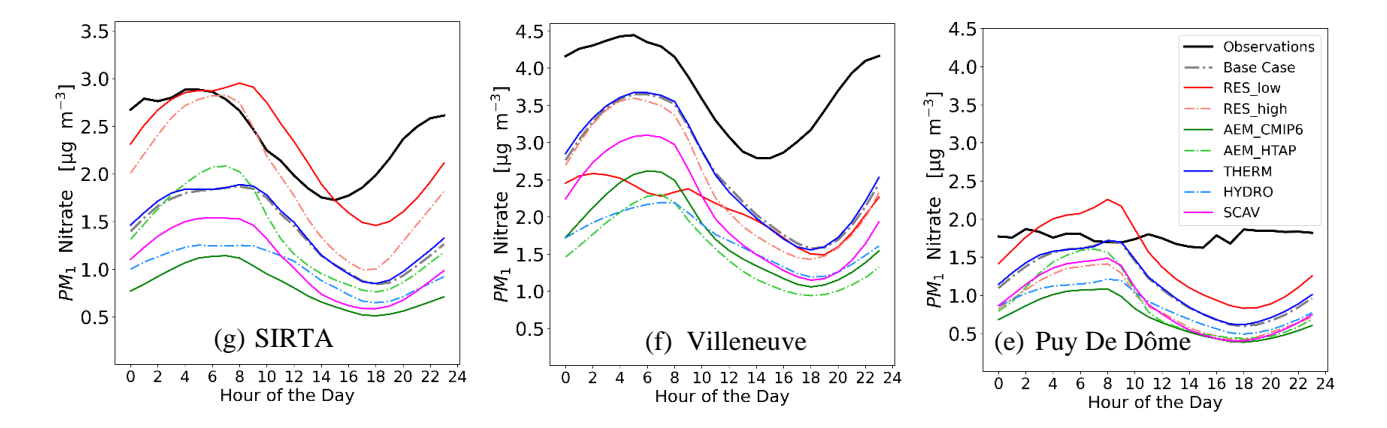
843



<u>Figure 8</u>: Diurnal evolution of measured (black lines) and predicted (colored lines) PM₁ NO₃-surface concentrations from the base case model and all model sensitivity cases for the stations at (a) Birkenes, (b) Bucharest, (c) Hohenpeissenberg and (d) Melpitz.







<u>Figure 8 (cont)</u>: Diurnal evolution of measured (black line) and predicted (colored lines) PM_1 NO_3^- surface concentrations from the base case model and all model sensitivity cases for the stations at (e) SIRTA, (f) Villeneuve and (g) Puy De Dôme.

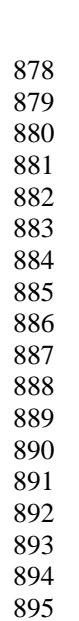
5.3 Tropospheric burden of particulate nitrate

The global tropospheric burden of aerosol nitrate, defined as the total amount (in Tg) present in the Earth's troposphere and averaged over the entire time period from 2008 to 2018, simulated by the base case and the sensitivity model runs is presented in Table 5 and Figure 9. The base case estimates a burden of 0.7 Tg, closely matching the multi-model average of 0.63 Tg reported by Bian et al. (2017). The 'RES_low' case gives the highest burden of 0.89 Tg, representing a 27% increase compared to the base case estimate. This is attributable to larger grid cells, which have a distorting effect on NOx concentration fields over broader regions, leading to elevated nocturnal production of particulate nitrate. Conversely, the 'RES_high' case exhibits the lowest burden of 0.53 Tg, a 24% decrease compared to the base case estimate, attributed to the more accurate reproduction of NOx concentration fields by this sensitivity and the reduced nocturnal production of particulate nitrate.

The 'CMIP' case estimates a burden close to the base case (0.74 Tg), while the 'HTAP' model run produces a higher burden of 0.88 Tg, driven by the higher NO_x emissions compared to the base case, particularly over India and the Western US. The 'THERM' and 'HYDRO' cases both yielded burdens of 0.69 Tg, indicating a minimal impact of the aerosol thermodynamic state assumption, as well as the N_2O_5 uptake coefficient for hydrolysis on the nitrate aerosol burden. The 'SCAV' case estimates a lower burden of 0.53 Tg due to the increased wet deposition rates from the simplified scavenging approach. This result is consistent with the results reported by Tost et al. (2007b), who calculated increased deposition rates using analogous simplifications and assumptions, including a pH of 5 for rain and clouds.







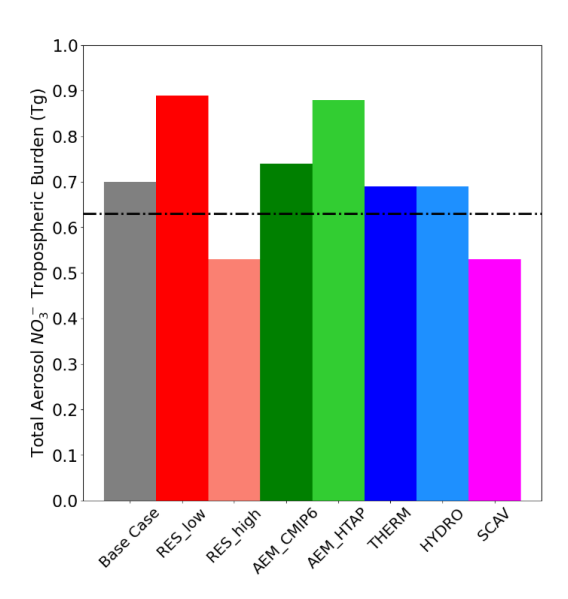


Figure 9: Bar chart showing the average tropospheric burden of total aerosol NO₃⁻ predicted from the base case and all sensitivity cases for the period 2010-2018. The dashed horizontal line shows the average tropospheric burden from 9 models taken from Bian et al. (2017), which is equal to 0.63 Tg.

<u>Table 5:</u> Average tropospheric burden of aerosol NO₃⁻ for the period 2010-2018 for the base case and all sensitivity simulations.

902
903

897 898

899

900

Simulation case	NO ₃ -Tropospheric Burden (Tg)
Base Case	0.70
RES_low (T42)	0.89
RES_high (T106)	0.53
CMIP6	0.74
НТАР	0.88
THERM	0.69
HYDRO	0.69
SCAV	0.53





6. Conclusions

This study investigated the impact of diverse atmospheric modeling components on the accuracy of the simulated surface concentrations of nitrate aerosols. A series of sensitivity scenarios were developed to assess the impact of grid resolution, anthropogenic emission inventories, aerosol thermodynamic assumptions, uptake coefficient for N_2O_5 hydrolysis, and scavenging treatments on model predictions. A comparative analysis was conducted against $PM_{2.5}$ filter observations and PM_1 AMS measurements, focusing on polluted regions within the Northern Hemisphere. The findings indicated that accurately replicating observed $PM_{2.5}$ and PM_1 concentrations requires a nuanced approach, as no single model configuration consistently yielded the best results for all conditions and regions.

For PM_{2.5} observations, the model performed best in the USA region, with the lowest overall bias and error metrics for all sensitivity simulations. In East Asia, the model consistently overpredicted concentrations in all configurations, although percentage differences were often moderate. Despite the significant model bias within this region, certain configurations improved the simulated concentrations and reduced the associated statistical metrics. These configurations included higher grid resolution, a lower uptake coefficient for N₂O₅ hydrolysis, and a simplified aerosol scavenging treatment. Conversely, Europe proved to be a particularly difficult region for the model to reproduce, with both under- and over-predictions of nitrate concentrations relative to observations, a pattern that showed significant seasonal variation. In particular, the simulated nitrate overprediction in Europe peaked during the summer. This discrepancy can be attributed to measurement artifacts under warm conditions and the enhanced evaporation of the semi-volatile nitrate aerosol species from the nylon filters used. This overprediction was also observed in North America when compared with nitrate observations from the EPA network. Conversely, the model showed increased discrepancies with the IMPROVE and EANET network observations during the colder periods. Despite these challenges, the scenarios that showed improvement over the base case predictions for East Asia were found to be equally effective in the other two regions, highlighting their importance in improving the accuracy of the model in reproducing PM_{2.5} nitrate observations.

For PM1 observations, the model performance varied significantly by the location type and region. In general, simulated urban nitrate was in best agreement with observations in all regions. However, rural observations were underpredicted in North America and strongly overpredicted in India. In contrast, rural observations in Europe and East Asia were more accurately reproduced by the base and CMIP cases, respectively. In general, downwind locations posed the greatest challenge to the model, with underprediction biases evident in Europe and North America, while the opposite behavior was observed for East Asia. Overall, the base case showed satisfactory agreement with most observations for the regions of Europe and East Asia. In contrast to the PM2.5 comparison, it was challenging to identify specific model configurations that consistently outperformed the base case in terms of predicted nitrate concentrations or statistical metrics. However, the choice of emission inventory proved to be the most important factor in improving model accuracy. Specifically, the model runs that used the CAMS database provided the best representation of particulate nitrate concentrations for Europe, the model runs that used the HTAPv3 database were most accurate for observations in North America, while the model runs that used the CMIP6 database best captured values in East Asia.

An analysis of the diurnal variation of PM₁ nitrate concentrations observed at European stations showed that the majority of model configurations effectively captured the general diurnal patterns of observations at most stations, with the exception of remote stations that lacked significant

https://doi.org/10.5194/egusphere-2025-313 Preprint. Discussion started: 12 February 2025 © Author(s) 2025. CC BY 4.0 License.





diurnal variation. However, the model results systematically over-emphasized the evening minima and showed a strong decrease in concentrations after midday. This behavior was not reflected in the observations, leading to under-predictions of the afternoon and evening observations. The choice of grid resolution proved to have the most significant impact on the predicted diurnal patterns. The high-resolution configuration showed a higher accuracy during the morning hours, while the lower-resolution configuration showed a better ability to capture afternoon and evening values. Among the emission inventories, the use of the CAMS database provided the most reliable estimates for PM₁ nitrate particle concentrations over Europe.

Finally, for the tropospheric nitrate aerosol burden, the base case, the metastable aerosol state assumption, the lower uptake coefficient for N_2O_5 hydrolysis, and the use of the CMIP6 emissions database resulted in values that were the closest to the multi-model average value reported by Bian et al. (2017). The scenarios with reduced grid resolution and the HTAPv3 emissions database resulted in estimates that were approximately 25% higher than the base case, reflecting the influence of the larger grid cells and the expanded precursor fields. Conversely, the scenarios where a higher grid resolution and a simplified aerosol scavenging treatment were used estimated burdens approximately 25% lower compared to the base case, attributable to the finer spatial resolution and increased wet deposition, respectively.

In conclusion, this study underscores the complexity of accurately modeling nitrate aerosols. The findings highlight the importance of selecting appropriate configurations based on regional and seasonal conditions, with high-resolution grids, CMIP6 emissions, and adjusted uptake coefficients for N_2O_5 hydrolysis being pivotal in improving the model performance. Nevertheless, the pronounced variability across regions and seasons shows the need for a flexible and adaptable approach to improving atmospheric modeling of particulate nitrate concentrations.





974 Code and Data Availability

- 975 The usage of MESSy (Modular Earth Submodel System) and access to the source code is licensed
- 976 to all affiliates of institutions which are members of the MESSy Consortium. Institutions can
- 977 become a member of the MESSy Consortium by signing the "MESSy Memorandum of
- 978 Understanding". More information can be found on the MESSy Consortium website:
- http://www.messy-interface.org (last access: 22 May 2024). The code used in this study has been
- 980 based on MESSy version 2.55 and is archived with a restricted access DOI
- 981 (https://doi.org/10.5281/zenodo.8379120, The MESSy Consortium, 2023). The data produced in
- the study is available from the authors upon request.

983

Acknowledgements

- This work was supported by the project FORCeS funded from the European Union's Horizon 2020
- 986 research and innovation program under grant agreement No 821205. The work described in this
- paper has received funding from the Initiative and Networking Fund of the Helmholtz Association
- 988 through the project "Advanced Earth System Modelling Capacity (ESM)". The authors gratefully
- 989 acknowledge the Earth System Modelling Project (ESM) for funding this work by providing
- omputing time on the ESM partition of the supercomputer JUWELS (Alvarez, 2021) at the Jülich
- 991 Supercomputing Centre (JSC).

992

993

984

Competing Interests

The authors declare that they have no competing interests.

995 996

Author Contributions

- 997 AM and VAK wrote the paper with contributions from APT, HF and SS. VAK and APT planned
- 998 the research. AM performed the simulations and analyzed the results, assisted by VAK and APT.
- 999 APT and SS provided the observational data. All the authors discussed the results and contributed
- 1000 to the paper.





REFERENCES

- Aksoyoglu, S., Ciarelli, G., El-Haddad, I., Baltensperger, U., and Prévôt, A. S. H.: Secondary inorganic aerosols in Europe: sources and the significant influence of biogenic VOC emissions, especially on ammonium nitrate, Atmospheric Chemistry and Physics, 17, 7757–7773, https://doi.org/10.5194/acp-17-7757-2017, 2017.
- Alvarez, D.: JUWELS cluster and booster: Exascale pathfinder with modular supercomputing architecture at juelich supercomputing Centre, Journal of large-scale research facilities JLSRF, 7, A183-A183, https://doi.org/10.17815/ilsrf-7-183, 2021.
- Ames, R. B. and Malm, W. C.: Comparison of sulfate and nitrate particle mass concentrations measured by IMPROVE and the CDN, Atmospheric Environment, 35, 905-916, https://doi.org/10.1016/S1352-2310(00)00369-1, 2001.
- Ansari, A. S. and Pandis, S. N.: The effect of metastable equilibrium states on the partitioning of nitrate between the gas and aerosol phases, Atmospheric Environment, 34, 157-168, https://doi.org/10.1016/S1352-2310(99)00242-3, 2000.
- Astitha, M., Lelieveld, J., Kader, M. A., Pozzer, A., and de Meij, A.: Parameterization of dust emissions in the global atmospheric chemistry-climate model EMAC: impact of nudging and soil properties, Atmospheric Chemistry and Physics, 12, 11057-11083, https://doi.org/10.5194/acp-12-11057-2012, 2012.
- Bacer, S., Sullivan, S. C., Karydis, V. A., Barahona, D., Kramer, M., Nenes, A., Tost, H., Tsimpidi, A. P., Lelieveld, J., and Pozzer, A.: Implementation of a comprehensive ice crystal formation parameterization for cirrus and mixed-phase clouds in the EMAC model (based on MESSy 2.53), Geoscientific Model Development , 11, https://doi.org/10.5194/gmd-11-4021-2018 , 2018.
- Bellouin, N., Rae, J., Jones, A., Johnson, C., Haywood, J., and Boucher, O.: Aerosol forcing in the Climate Model Intercomparison Project (CMIP5) simulations by HadGEM2-ES and the role of ammonium nitrate, Journal of Geophysical Research: Atmospheres, 116, https://doi.org/10.1029/2011JD016074, 2011.
- Bertram, T. H., Thornton, J. A., Riedel, T. P., Middlebrook, A. M., Bahreini, R., Bates, T. S., Quinn, P. K., & Coffman, D. J.: Direct observations of N₂O₅ reactivity on ambient aerosol particles, Geophysical Research Letters, 36, https://doi.org/10.1029/2009GL040248, 2009.
- Bian, H., Chin, M., Hauglustaine, D. A., Schulz, M., Myhre, G., Bauer, S. E., Lund, M. T., Karydis, V. A., Kucsera, T. L., Pan, X., Pozzer, A., Skeie, R. B., Steenrod, S. D., Sudo, K., Tsigaridis, K., Tsimpidi, A. P., and Tsyro, S. G.: Investigation of global particulate nitrate from the AeroCom phase III experiment, Atmospheric Chemistry and Physics, 17, 12911–12940, https://doi.org/10.5194/acp-17-12911-2017, 2017.
- Bouwman, A. F., Lee, D. S., Asman, W. A., Dentener, F. J., Van Der Hoek, K. W., and Olivier, J. G. J.: A global high-resolution emission inventory for ammonia, Global biogeochemical cycles, 11, 561-587, https://doi.org/10.1029/97GB02266, 1997.
- Bromley, L. A.: Thermodynamic properties of strong electrolytes in aqueous solutions, AIChE journal, 19, 313-320, https://doi.org/10.1002/aic.690190216, 1973.
- Brown, S.S., Dubé, W.P., Fuchs, H., Ryerson, T.B., Wollny, A.G., Brock, C.A., Bahreini, R., Middlebrook, A.M., Neuman, J.A., Atlas, E. and Roberts, J.M.,: Reactive uptake coefficients for N₂O₅ determined from aircraft measurements during the Second Texas Air Quality Study: Comparison to current model parameterizations, Journal of Geophysical Research: Atmospheres, 114, https://doi.org/10.1029/2008JD011679, 2009.
- 1046 Chang, W. L., Bhave, P. V., Brown, S. S., Riemer, N., Stutz, J., & Dabdub, D.: Heterogeneous atmospheric chemistry, ambient measurements, and model calculations of N_2O_5 : A review, Aerosol Science and Technology, 45, 665-695, https://doi.org/10.1080/02786826.2010.551672, 2011.





- 1049 Chang, W.L., Brown, S.S., Stutz, J., Middlebrook, A.M., Bahreini, R., Wagner, N.L., Dubé, W.P., Pollack, 1050 I.B., Ryerson, T.B. and Riemer, N.,: Evaluating N_2O_5 heterogeneous hydrolysis parameterizations 1051 for CalNex 2010, Journal of Geophysical Research: Atmospheres, 121, 5051-5070, https://doi.org/10.1002/2015JD024737, 2016.
 - Chen, Y., Wolke, R., Ran, L., Birmili, W., Spindler, G., Schröder, W., Su, H., Cheng, Y., Tegen, I., and Wiedensohler, A.: A parameterization of the heterogeneous hydrolysis of N₂O₅ for mass-based aerosol models: improvement of particulate nitrate prediction, Atmospheric Chemistry and Physics, 18, 673–689, https://doi.org/10.5194/acp-18-673-2018, 2018.
 - Chowdhury, S., Pozzer, A., Haines, A., Klingmueller, K., Münzel, T., Paasonen, P., Sharma, A., Venkataraman, C. and Lelieveld, J.,: Global health burden of ambient PM2. 5 and the contribution of anthropogenic black carbon and organic aerosols, Environment International, 159, 107020, https://doi.org/10.1016/j.envint.2021.107020, 2022.
 - Crippa, M., Guizzardi, D., Butler, T., Keating, T., Wu, R., Kaminski, J., Kuenen, J., Kurokawa, J., Chatani, S., Morikawa, T., Pouliot, G., Racine, J., Moran, M. D., Klimont, Z., Manseau, P. M., Mashayekhi, R., Henderson, B. H., Smith, S. J., Suchyta, H., Muntean, M., Solazzo, E., Banja, M., Schaaf, E., Pagani, F., Woo, J.-H., Kim, J., Monforti-Ferrario, F., Pisoni, E., Zhang, J., Niemi, D., Sassi, M., Ansari, T., and Foley, K.: The HTAP_v3 emission mosaic: merging regional and global monthly emissions (2000–2018) to support air quality modelling and policies, Earth Sysem Science Data, 15, 2667–2694, https://doi.org/10.5194/essd-15-2667-2023, 2023.
 - Dee, D. P., Uppala, S. M., Simmons, A. J., Berrisford, P., Poli, P., Kobayashi, S., Andrae, U., Balmaseda, M. A., Balsamo, G., Bauer, P., Bechtold, P., Beljaars, A. C. M., van de Berg, L., Bidlot, J., Bormann, N., Delsol, C., Dragani, R., Fuentes, M., Geer, A. J., Haimberger, L., Healy, S. B., Hersbach, H., Hólm, E. V., Isaksen, L., Kållberg, P., Köhler, M., Matricardi, M., McNally, A. P., Monge-Sanz, B. M., Morcrette, J. J., Park, B. K., Peubey, C., de Rosnay, P., Tavolato, C., Thépaut, J. N., and Vitart, F.: The ERA-Interim reanalysis: configuration and performance of the data assimilation system, Journal of the Royal Meteorological 137, 553-597, Quarterly Society, https://doi.org/10.1002/qj.828, 2011.
 - Dentener, F., Kinne, S., Bond, T., Boucher, O., Cofala, J. and co-authors: Emissions of primary aerosol and precursor gases in the years 2000 and 1750 prescribed data-sets for AeroCom, Atmospheric Chemistry and Physics, 6, 4321-4344, https://doi.org/10.5194/acp-6-4321-2006, 2006.
 - Docherty, K. S., Aiken, A. C., Huffman, J. A., Ulbrich, I. M., DeCarlo, P. F., Sueper, D., Worsnop, D. R., Snyder, D. C., Peltier, R. E., Weber, R. J., Grover, B. D., Eatough, D. J., Williams, B. J., Goldstein, A. H., Ziemann, P. J., and Jimenez, J. L.: The 2005 Study of Organic Aerosols at Riverside (SOAR-1): instrumental intercomparisons and fine particle composition, Atmospheric Chemistry and Physics, 11, 12387–12420, https://doi.org/10.5194/acp-11-12387-2011, 2011.
 - EMEP Programme Air Pollutant Monitoring Data, available at: https://projects.nilu.no/ccc/index.html
 Evans, M. J. and Jacob, D. J.: Impact of new laboratory studies of N₂O₅ hydrolysis on global model budgets of tropospheric nitrogen oxides, ozone, and OH, Geophysical Research Letters, 32, https://doi.org/10.1029/2005GL022469, 2005.
 - Fountoukis, C. and Nenes, A.: ISORROPIA II: a computationally efficient thermodynamic equilibrium model for K+–Ca 2+–Mg 2+–NH 4+–Na+–SO 4 2-–NO 3-–Cl-–H 2 O aerosols, Atmospheric Chemistry and Physics, 7, 4639-4659, https://doi.org/10.5194/acp-7-4639-2007, 2007.
 - Fountoukis, C., Nenes, A., Sullivan, A., Weber, R., Van Reken, T., Fischer, M., Matías, E., Moya, M., Farmer, D., and Cohen, R. C.: Thermodynamic characterization of Mexico City aerosol during MILAGRO 2006, Atmospheric Chemistry and Physics, 9, 2141-2156, https://doi.org/10.5194/acp-9-2141-2009, 2009.
 - Ge, X., Schaap, M., Kranenburg, R., Segers, A., Reinds, G. J., Kros, H., and de Vries, W.: Modeling atmospheric ammonia using agricultural emissions with improved spatial variability and temporal





- dynamics, Atmospheric Chemistry and Physics, 20, 16055–16087, https://doi.org/10.5194/acp-1098 20-16055-2020 , 2020.
 - Glantz, P., Fawole, O. G., Ström, J., Wild, M., & Noone, K. J.: Unmasking the effects of aerosols on greenhouse warming over Europe, Journal of Geophysical Research: Atmospheres, 127, e2021JD035889, https://doi.org/10.1029/2021JD035889, 2022.
 - Grewe, V., Brunner, D., Dameris, M., Grenfell, J. L., Hein, R., Shindell, D., and Staehelin, J.: Origin and variability of upper tropospheric nitrogen oxides and ozone at northern mid-latitudes, Atmospheric Environment, 35, 3421-3433, https://doi.org/10.1016/S1352-2310(01)00134-0, 2001.
 - Guelle, W., Schulz, M., Balkanski, Y., & Dentener, F.: Influence of the source formulation on modeling the atmospheric global distribution of sea salt aerosol, Journal of Geophysical Research: Atmospheres, 106, 27509-27524, https://doi.org/10.1029/2001JD900249, 2001.
 - Guo, H., Sullivan, A. P., Campuzano-Jost, P., Schroder, J. C., Lopez-Hilfiker, F. D., Dibb, J. E., Jimenez, J. L., Thornton, J. A., Brown, S. S., Nenes, A., and Weber, R. J.: Fine particle pH and the partitioning of nitric acid during winter in the northeastern United States, Journal of Geophysical Research: Atmospheres, 121, 10, 355-310, 376, https://doi.org/10.1002/2016JD025311, 2016.
 - Hauglustaine, D. A., Balkanski, Y., and Schulz, M.: A global model simulation of present and future nitrate aerosols and their direct radiative forcing of climate, Atmospheric Chemistry and Physics, 14, 11031-11063, https://doi.org/10.5194/acp-14-11031-2014, 2014.
 - Heald, C. L., Collett Jr., J. L., Lee, T., Benedict, K. B., Schwandner, F. M., Li, Y., Clarisse, L., Hurtmans, D. R., Van Damme, M., Clerbaux, C., Coheur, P.-F., Philip, S., Martin, R. V., and Pye, H. O. T.: Atmospheric ammonia and particulate inorganic nitrogen over the United States, Atmospheric Chemistry and Physics, 12, 10295–10312, https://doi.org/10.5194/acp-12-10295-2012, 2012.
 - Hendriks, C., Kranenburg, R., Kuenen, J. J. P., Van den Bril, B., Verguts, V., & Schaap, M.: Ammonia emission time profiles based on manure transport data improve ammonia modelling across north western Europe. Atmospheric Environment, 131, 83-96, https://doi.org/10.1016/j.atmosenv.2016.01.043, 2016.
 - Im, U., Bauer, S. E., Frohn, L. M., Geels, C., Tsigaridis, K., & Brandt, J.: Present-day and future PM2. 5 and O3-related global and regional premature mortality in the EVAv6. 0 health impact assessment model, Environmental Research, 216, 114702, https://doi.org/10.1016/j.envres.2022.114702, 2023.
 - Inness, A., Ades, M., Agustí-Panareda, A., Barré, J., Benedictow, A., Blechschmidt, A.-M., Dominguez, J. J., Engelen, R., Eskes, H., Flemming, J., Huijnen, V., Jones, L., Kipling, Z., Massart, S., Parrington, M., Peuch, V.-H., Razinger, M., Remy, S., Schulz, M., and Suttie, M.: The CAMS reanalysis of atmospheric composition, Atmospheric Chemistry and Physics, 19, 3515–3556, https://doi.org/10.5194/acp-19-3515-2019, 2019.
 - Interagency Monitoring of Protected Visual Environment (IMPROVE), available at http://vista.cira.colostate.edu/lmprove/improve-data/
 - Jockel, P., Sander, R., Kerkweg, A., Tost, H., and Lelieveld, J.: the modular earth submodel system (MESSy)-a new approach towards earth system modeling, Atmospheric Chemistry and Physics, 5, 433-444, https://doi.org/10.5194/acp-5-433-2005, 2005.
 - Jockel, P., Tost, H., Pozzer, A., Bruhl, C., Buchholz, J. and co-authors: The atmospheric chemistry general circulation model ECHAM5/MESSy1: consistent simulation of ozone from the surface to the mesosphere, Atmospheric Chemistry and Physics, 6, 5067-5104, https://doi.org/10.5194/acp-6-5067-2006, 2006.
- Jockel, P., Tost, H., Pozzer, A., Kunze, M., Kirner, O. and co-authors: Earth system chemistry integrated modelling (ESCiMo) with the modular earth submodel system (MESSy) version 2.51, Geoscientific Model Development, 9, 1153-1200, https://doi.org/10.5194/gmd-9-1153-2016, 2016.





- Jones, A. C., Hill, A., Remy, S., Abraham, N. L., Dalvi, M., Hardacre, C., Hewitt, A. J., Johnson, B., Mulcahy, J. P., and Turnock, S. T.: Exploring the sensitivity of atmospheric nitrate concentrations to nitric acid uptake rate using the Met Office's Unified Model, Atmospheric Chemistry and Physics, 21, 15901–15927, https://doi.org/10.5194/acp-21-15901-2021, 2021.
 - Kakavas, S., & Pandis, S. N.: Effects of urban dust emissions on fine and coarse PM levels and composition, Atmospheric Environment, 246, 118006, https://doi.org/10.1016/j.atmosenv.2020.118006 , 2021.
 - Karydis, V. A., Tsimpidi, A. P., Fountoukis, C., Nenes, A., Zavala, M., Lei, W. F., Molina, L. T., and Pandis, S. N.: Simulating the fine and coarse inorganic particulate matter concentrations in a polluted megacity, Atmospheric Environment, 44, 608-620 , https://doi.org/10.1016/j.atmosenv.2009.11.023, 2010.
 - Karydis, V. A., Tsimpidi, A. P., Lei, W., Molina, L. T., and Pandis, S. N.: Formation of semivolatile inorganic aerosols in the Mexico City Metropolitan Area during the MILAGRO campaign, Atmospheric Chemistry and Physics, 11, 13305-13323, https://doi.org/10.5194/acp-11-13305-2011, 2011.
 - Karydis, V. A., Tsimpidi, A. P., Pozzer, A., Astitha, M., and Lelieveld, J.: Effects of mineral dust on global atmospheric nitrate concentrations, Atmospheric Chemistry and Physics, 16, 1491-1509, https://doi.org/10.5194/acp-16-1491-2016, 2016.
 - Karydis, V. A., Tsimpidi, A. P., Bacer, S., Pozzer, A., Nenes, A., and Lelieveld, J.: Global impact of mineral dust on cloud droplet number concentration, Atmospheric Chemistry and Physics, 17, 5601-5621, https://doi.org/10.5194/acp-17-5601-2017, 2017.
 - Karydis, V. A., Tsimpidi, A. P., Pozzer, A., and Lelieveld, J.: How alkaline compounds control atmospheric aerosol particle acidity, Atmospheric Chemistry and Physics, 21, 14983-15001, https://doi.org/10.5194/acp-21-14983-2021, 2021.
 - Kerkweg, A., Sander, R., Tost, H., and Jöckel, P.: Technical note: Implementation of prescribed (OFFLEM), calculated (ONLEM), and pseudo-emissions (TNUDGE) of chemical species in the Modular Earth Submodel System (MESSy), Atmospheric Chemistry and Physics, 6, 3603–3609, https://doi.org/10.5194/acp-6-3603-2006, 2006a.
 - Kerkweg, A., Buchholz, J., Ganzeveld, L., Pozzer, A., Tost, H., and Jöckel, P.: An implementation of the dry removal processes DRY DEPosition and SEDImentation in the Modular Earth Submodel System (MESSy), Atmospheric Chemistry and Physics, 6, 4617-4632, https://doi.org/10.5194/acp-6-4617-2006, 2006b.
 - Klingmüller, K., Metzger, S., Abdelkader, M., Karydis, V. A., Stenchikov, G. L., Pozzer, A., and Lelieveld, J.: Revised mineral dust emissions in the atmospheric chemistry-climate model EMAC (MESSy 2.52 DU_Astitha1 KKDU2017 patch), Geoscientific Model Development, 11, 989-1008, https://doi.org/10.5194/gmd-11-989-2018, 2018.
 - Klingmuller, K., Lelieveld, J., Karydis, V. A., and Stenchikov, G. L.: Direct radiative effect of dust-pollution interactions, Atmospheric Chemistry and Physics, 19, 7397-7408, https://doi.org/10.5194/acp-19-7397-2019, 2019.
 - Klingmüller, K., Karydis, V. A., Bacer, S., Stenchikov, G. L., and Lelieveld, J.: Weaker cooling by aerosols due to dust-pollution interactions, Atmospheric Chemistry and Physics, 20, 15285-15295, https://doi.org/10.5194/acp-20-15285-2020, 2020.
 - Kok, J. F., Storelvmo, T., Karydis, V. A., Adebiyi, A. A., Mahowald, N. M., Evan, A. T., He, C. L., and Leung, D. M.: Mineral dust aerosol impacts on global climate and climate change, Nature Reviews Earth & Environment, 4, 71-86, https://doi.org/10.1038/s43017-022-00379-5, 2023.
- 1189 Kusik, C. L. and Meissner H.P.: Electrolyte Activity Coefficients in Inorganic Processing, AIChE Symp. Series, 173, 14-20, 1978.
- Lanz, V. A., Prévôt, A. S. H., Alfarra, M. R., Weimer, S., Mohr, C., DeCarlo, P. F., Gianini, M. F. D., Hueglin, C., Schneider, J., Favez, O., D'Anna, B., George, C., and Baltensperger, U.: Characterization of





- aerosol chemical composition with aerosol mass spectrometry in Central Europe: an overview, Atmospheric Chemistry and Physics, 10, 10453–10471, https://doi.org/10.5194/acp-10-10453-2010, 2010.
 - Li, S., Zhang, F., Jin, X., Sun, Y., Wu, H., Xie, C., Chen, L., Liu, J., Wu, T., Jiang, S. and Cribb, M.,: Characterizing the ratio of nitrate to sulfate in ambient fine particles of urban Beijing during 2018–2019, Atmospheric environment, 237, 117662, https://doi.org/10.1016/j.atmosenv.2020.117662, 2020.
 - Liu, L., Bei, N., Hu, B., Wu, J., Liu, S., Li, X., Wang, R., Liu, Z., Shen, Z. and Li, G.,: Wintertime nitrate formation pathways in the north China plain: Importance of N₂O₅ heterogeneous hydrolysis, Environmental Pollution, 266, 115287, https://doi.org/10.1016/j.envpol.2020.115287. 2020.
 - Lohmann, U. and Ferrachat, S.: Impact of parametric uncertainties on the present-day climate and on the anthropogenic aerosol effect, Atmospheric Chemistry and Physics, 10, https://doi.org/10.5194/acp-10-11373-2010, 2010.
 - Meissner, H. P. and Peppas, N. A.: Activity coefficients aqueous solutions of polybasic acids and their salts, AIChE Journal, 19, 806–809, https://doi.org/10.1002/aic.690190419, 1973.
 - Metzger, S., Dentener, F., Krol, M., Jeuken, A., & Lelieveld, J.: Gas/aerosol partitioning 2. Global modeling results, Journal of Geophysical Research: Atmospheres, 107, ACH-17, https://doi.org/10.1029/2001JD001103, 2002.
 - Miao, R., Chen, Q., Zheng, Y., Cheng, X., Sun, Y., Palmer, P. I., Shrivastava, M., Guo, J., Zhang, Q., Liu, Y., Tan, Z., Ma, X., Chen, S., Zeng, L., Lu, K., and Zhang, Y.: Model bias in simulating major chemical components of PM_{2.5} in China, Atmospheric Chemistry and Physics, 20, 12265–12284, https://doi.org/10.5194/acp-20-12265-2020, 2020.
 - Milousis, A., Tsimpidi, A. P., Tost, H., Pandis, S. N., Nenes, A., Kiendler-Scharr, A., and Karydis, V. A.: Implementation of the ISORROPIA-lite aerosol thermodynamics model into the EMAC chemistry climate model (based on MESSy v2.55): implications for aerosol composition and acidity, Geoscientific Model Development, 17, 1111-1131, https://doi.org/10.5194/gmd-17-1111-2024, 2024.
 - Milousis, A., Klingmüller, K., Tsimpidi, A. P., Kok, J. F., Kanakidou, M., Nenes, A., and Karydis, V. A.: Impact of mineral dust on the global nitrate aerosol direct and indirect radiative effect, EGUsphere [preprint], https://doi.org/10.5194/egusphere-2024-1579, 2024.
 - Myhre, G., Samset, B. H., Schulz, M., Balkanski, Y., Bauer, S., Berntsen, T. K., Bian, H., Bellouin, N., Chin, M., Diehl, T., Easter, R. C., Feichter, J., Ghan, S. J., Hauglustaine, D., Iversen, T., Kinne, S., Kirkevåg, A., Lamarque, J. F., Lin, G., Liu, X., Lund, M. T., Luo, G., Ma, X., van Noije, T., Penner, J. E., Rasch, P. J., Ruiz, A., Seland, Ø., Skeie, R. B., Stier, P., Takemura, T., Tsigaridis, K., Wang, P., Wang, Z., Xu, L., Yu, H., Yu, F., Yoon, J. H., Zhang, K., Zhang, H., and Zhou, C.: Radiative forcing of the direct aerosol effect from AeroCom Phase II simulations, Atmospheric Chemistry and Physics, 13, 1853-1877, https://doi.org/10.5194/acp-13-1853-2013, 2013.
 - Nair, A. A., & Yu, F.: Quantification of atmospheric ammonia concentrations: A review of its measurement and modeling, Atmosphere, 11, 1092, https://doi.org/10.3390/atmos11101092, 2020.
- Nair, H. R. C. R., Budhavant, K., Manoj, M. R., Andersson, A., Satheesh, S. K., Ramanathan, V., & Gustafsson, Ö.: Aerosol demasking enhances climate warming over South Asia, NPJ climate and atmospheric science, 6, 39, https://doi.org/10.1038/s41612-023-00367-6, 2023.
- Nenes, A., Pandis, S. N., Weber, R. J., and Russell, A.: Aerosol pH and liquid water content determine when particulate matter is sensitive to ammonia and nitrate availability, Atmospheric Chemistry and Physics, 20, 3249-3258, https://doi.org/10.5194/acp-20-3249-2020, 2020.





- 1240 O'Neill, B. C., Tebaldi, C., van Vuuren, D. P., Eyring, V., Friedlingstein, P., Hurtt, G., Knutti, R., Kriegler, E., Lamarque, J.-F., Lowe, J., Meehl, G. A., Moss, R., Riahi, K., and Sanderson, B. M.: The Scenario Model Intercomparison Project (ScenarioMIP) for CMIP6, Geoscientific Model Development, 9, 3461–3482, https://doi.org/10.5194/gmd-9-3461-2016, 2016.
 - Phillips, G. J., Thieser, J., Tang, M., Sobanski, N., Schuster, G., Fachinger, J., Drewnick, F., Borrmann, S., Bingemer, H., Lelieveld, J., and Crowley, J. N.: Estimating N₂O₅ uptake coefficients using ambient measurements of NO₃, N₂O₅, ClNO₂ and particle-phase nitrate, Atmospheric Chemistry and Physics, 16, 13231–13249, https://doi.org/10.5194/acp-16-13231-2016, 2016.
 - Pinder, R. W., Adams, P. J., Pandis, S. N., & Gilliland, A. B.: Temporally resolved ammonia emission inventories: Current estimates, evaluation tools, and measurement needs, Journal of Geophysical Research: Atmospheres, 111, https://doi.org/10.1029/2005JD006603, 2006.
 - Pozzer, A., Jöckel, P., Sander, R., Williams, J., Ganzeveld, L., and Lelieveld, J.: The MESSy-submodel AIRSEA calculating the air-sea exchange of chemical species, Atmospheric Chemistry and Physics, 6, 5435-5444, https://doi.org/10.5194/acp-6-5435-2006, 2006.
 - Pringle, K. J., Tost, H., Message, S., Steil, B., Giannadaki, D., Nenes, A., Fountoukis, C., Stier, P., Vignati, E., and Leieved, J.: Description and evaluation of GMXe: a new aerosol submodel for global simulations (v1), Geoscientific Model Development, 3, https://doi.org/10.5194/gmd-3-391-2010, 2010a.
 - Pringle, K. J., Tost, H., Metzger, S., Steil, B., Giannadaki, D., Nenes, A., Fountoukis, C., Stier, P., Vignati, E., and Lelieveld, J.: Corrigendum to "Description and evaluation of GMXe: a new aerosol submodel for global simulations (v1)" published in Geoscientific Model Development, 3, 391–412, 2010, Geoscientific Model Development, 3(2), 413-413, https://doi.org/10.5194/gmd-3-413-2010, 2010b.
 - Pye, H. O. T., Nenes, A., Alexander, B., Ault, A. P., Barth, M. C., Clegg, S. L., Collett Jr., J. L., Fahey, K. M., Hennigan, C. J., Herrmann, H., Kanakidou, M., Kelly, J. T., Ku, I.-T., McNeill, V. F., Riemer, N., Schaefer, T., Shi, G., Tilgner, A., Walker, J. T., Wang, T., Weber, R., Xing, J., Zaveri, R. A., and Zuend, A.: The acidity of atmospheric particles and clouds, Atmospheric Chemistry and Physics, 20, 4809–4888, https://doi.org/10.5194/acp-20-4809-2020, 2020.
 - Qu, Y., Chen, Y., Liu, X., Zhang, J., Guo, Y., & An, J.: Seasonal effects of additional HONO sources and the heterogeneous reactions of N_2O_5 on nitrate in the North China Plain, Science of the Total Environment, 690, 97-107, https://doi.org/10.1016/j.scitotenv.2019.06.436, 2019.
 - Randerson, J.T., G.R. van der Werf, L. Giglio, G.J. Collatz, and P.S. Kasibhatla: Global Fire Emissions Database, Version 4.1 (GFEDv4). ORNL DAAC, Oak Ridge, Tennessee, USA. https://doi.org/10.3334/ORNLDAAC/1293, 2017.
 - Reis, S., Pinder, R. W., Zhang, M., Lijie, G., and Sutton, M. A.: Reactive nitrogen in atmospheric emission inventories, Atmospheric Chemistry and Physics, 9, 7657–7677, https://doi.org/10.5194/acp-9-7657-2009, 2009.
 - Roeckner, E., Brokopf, R., Esch, M., Giorgetta, M., Hagemann, S., Kornblueh, L., Manzini, E., Schlese, U., and Schulzweida, U.: Sensitivity of simulated climate to horizontal and vertical resolution in the ECHAM5 atmosphere model, Journal of Climate, 19, 3771-3791, https://doi.org/10.1175/JCLI3824.1, 2006.
 - Sander, R., Baumgaertner, A., Cabrera-Perez, D., Frank, F., Gromov, S., Grooss, J. U., Harder, H., Huijnen, V., Jockel, P., Karydis, V. A., Niemeyer, K. E., Pozzer, A., Hella, R. B., Schultz, M. G., Taraborrelli, D., and Tauer, S.: The community atmospheric chemistry box model CAABA/MECCA-4.0, Geoscientific Model Development, 12, 1365-1385, https://doi.org/10.5194/gmd-12-1365-2019, 2019.
 - Schaap, M., van Loon, M., ten Brink, H. M., Dentener, F. J., and Builtjes, P. J. H.: Secondary inorganic aerosol simulations for Europe with special attention to nitrate, Atmospheric Chemistry and Physics, 4, 857–874, https://doi.org/10.5194/acp-4-857-2004, 2004.

https://doi.org/10.5194/egusphere-2025-313 Preprint. Discussion started: 12 February 2025 © Author(s) 2025. CC BY 4.0 License.





- Seinfeld, J. H. and Pandis, S. N.: Atmospheric chemistry and physics: from air pollution to climate change.

 John Wiley & Sons, ISBN 1118947401, 2016.
 - Song, S., Gao, M., Xu, W., Shao, J., Shi, G., Wang, S. and co-authors: Fine-particle pH for Beijing winter haze as inferred from different thermodynamic equilibrium models, Atmospheric Chemistry and Physics, 18, 7423-7438, https://doi.org/10.5194/acp-18-7423-2018, 2018.
 - Stier, P., Feichter, J., Kinne, S., Kloster, S., Vignati, E., Wilson, J., Ganzeveld, L., Tegen, I., Werner, M., Balkanski, Y., Schulz, M., Boucher, O., Minikin, A., and Petzold, A.: The aerosol-climate model ECHAM5-HAM, Atmospheric Chemistry and Physics, 5, 1125–1156, https://doi.org/10.5194/acp-5-1125-2005, 2005.
 - Storelvmo, T., Leirvik, T., Lohmann, U., Phillips, P. C., & Wild, M.: Disentangling greenhouse warming and aerosol cooling to reveal Earth's climate sensitivity, Nature Geoscience, 9, 286-289, https://doi.org/10.1038/ngeo2670, 2016.
 - Sutton, M. A., Reis, S., Riddick, S. N., Dragosits, U., Nemitz, E., Theobald, M. R., Tang, Y. S., Braban, C. F., Vieno, M., Dore, A. J., Mitchell, R. F., Wanless, S., Daunt, F., Fowler, D., Blackall, T. D., Milford, C., Flechard, C. R., Loubet, B., Massad, R., Cellier, P., Personne, E., Coheur, P. F., Clarisse, L., Van Damme, M., Ngadi, Y., Clerbaux, C., Skjøth, C. A., Geels, C., Hertel, O., Wichink Kruit, R. J., Pinder, R. W., Bash, J. O., Walker, J. T., Simpson, D., Horváth, L., Misselbrook, T. H., Bleeker, A., Dentener, F., and de Vries, W.: Towards a climate-dependent paradigm of ammonia emission and deposition, Philosophical Transactions of the Royal Society B: Biological Sciences, 368, https://doi.org/10.1098/rstb.2013.0166, 2013.
 - The Acid Deposition Monitoring Network in East Asia, available at https://monitoring.eanet.asia/document/public/index
 - Tilgner, A., Schaefer, T., Alexander, B., Barth, M., Collett Jr., J. L., Fahey, K. M., Nenes, A., Pye, H. O. T., Herrmann, H., and McNeill, V. F.: Acidity and the multiphase chemistry of atmospheric aqueous particles and clouds, Atmospheric Chemistry and Physics, 21, 13483–13536, https://doi.org/10.5194/acp-21-13483-2021, 2021.
 - Tost, H., Jockel, P. J., Kerkweg, A., Sander, R., and Lelieveld, J.: Technical note: A new comprehensive SCAVenging submodel for global atmospheric chemistry modelling, Atmospheric Chemistry and Physics, 6, 565-574, https://doi.org/10.5194/acp-6-565-2006, 2006.
 - Tost, H., Jöckel, P., and Lelieveld, J.: Lightning and convection parameterisations uncertainties in global modelling, Atmospheric Chemistry and Physics, 7, 4553-4568, https://doi.org/10.5194/acp-7-4553-2007, 2007a.
 - Tost, H., Jockel, P., Kerkweg, A., Pozzer, A., Sander, R., and Lelieveld, J.: Global cloud and precipitation chemistry and wet deposition: tropospheric model simulations with ECHAM5/MESSy1, Atmospheric Chemistry and Physics, 7, 2733-2757, https://doi.org/10.5194/acp-7-2733-2007, 2007b.
 - Tsimpidi, A. P., Karydis, V. A., and Pandis, S. N.: Response of inorganic fine particulate matter to emission changes of sulfur dioxide and ammonia: The eastern United States as a case study, J. Air Waste Manage. Assoc., 57, 1489-1498, https://doi.org/10.3155/1047-3289.57.12.1489, 2007.
 - Tsimpidi, A. P., Karydis, V. A., and Pandis, S. N.: Response of Fine Particulate Matter to Emission Changes of Oxides of Nitrogen and-Anthropogenic Volatile Organic Compounds in the Eastern United States, J. Air Waste Manage. Assoc., 58, 1463-1473, https://doi.org/10.3155/1047-3289.58.11.1463, 2008.
- Tsimpidi, A. P., Trail, M., Hu, Y. T., Nenes, A., and Russell, A. G.: Modeling an air pollution episode in northwestern United States: Identifying the effect of nitrogen oxide and volatile organic compound emission changes on air pollutants formation using direct sensitivity analysis, J. Air Waste Manage. Assoc., 62, 1150-1165, https://doi.org/10.1080/10962247.2012.697093, 2012.





- Tsimpidi, A. P., Karydis, V. A., Pozzer, A., Pandis, S. N., and Lelieveld, J.: ORACLE (v1. 0): module to simulate the organic aerosol composition and evolution in the atmosphere, Geoscientific Model Development, 7, 3153-3172, https://doi.org/10.5194/gmd-7-3153-2014, 2014.
 - Tsimpidi, A. P., Karydis, V. A., Pandis, S. N., and Lelieveld, J.: Global combustion sources of organic aerosols: model comparison with 84 AMS factor-analysis data sets, Atmospheric Chemistry and Physics, 16, 8939–8962, https://doi.org/10.5194/acp-16-8939-2016, 2016.
 - Tsimpidi, A. P., Karydis, V. A., Pandis, S. N., and Lelieveld, J.: Global-scale combustion sources of organic aerosols: sensitivity to formation and removal mechanisms, Atmospheric Chemistry and Physics, 17, 7345-7364, https://doi.org/10.5194/acp-17-7345-2017, 2017.
 - Tsimpidi, A. P., Karydis, V. A., Pozzer, A., Pandis, S. N., and Lelieveld, J.: ORACLE 2-D (v2.0): an efficient module to compute the volatility and oxygen content of organic aerosol with a global chemistry–climate model, Geoscientific Model Development, 11, 3369-3389, https://doi.org/10.5194/gmd-11-3369-2018, 2018.
 - Tsimpidi, A. P., Scholz, S. M. C., Milousis, A., Mihalopoulos, N., and Karydis, V. A.: Aerosol Composition Trends during 2000–2020: In depth insights from model predictions and multiple worldwide observation datasets, EGUsphere [preprint], https://doi.org/10.5194/egusphere-2024-3590, 2024.
 - U.S. Environmental Protection Agency Clean Air Markets Division Clean Air Status and Trends Network (CASTNET), available at: https://www.epa.gov/castnet
 - Vignati, E., Wilson, J., and Stier, P.: M7: An efficient size-resolved aerosol microphysics module for large-scale aerosol transport models, Journal of Geophysical Research: Atmospheres, 109, https://doi.org/10.1029/2003JD004485, 2004.
 - Walker, J. M., Philip, S., Martin, R. V., and Seinfeld, J. H.: Simulation of nitrate, sulfate, and ammonium aerosols over the United States, Atmospheric Chemistry and Physics, 12, 11213–11227, https://doi.org/10.5194/acp-12-11213-2012, 2012.
 - Wang, H., Chen, X., Lu, K., Tan, Z., Ma, X., Wu, Z., Li, X., Liu, Y., Shang, D., Wu, Y. and Zeng, L.,: Wintertime N_2O_5 uptake coefficients over the North China Plain, Science bulletin, 65, 765-774, https://doi.org/10.1016/j.scib.2020.02.006, 2020.
 - Wang, Y., Zhang, Q. Q., He, K., Zhang, Q., and Chai, L.: Sulfate-nitrate-ammonium aerosols over China: response to 2000–2015 emission changes of sulfur dioxide, nitrogen oxides, and ammonia, Atmospheric Chemistry and Physics, 13, 2635–2652, https://doi.org/10.5194/acp-13-2635-2013, 2013.
 - Xie, X., Hu, J., Qin, M., Guo, S., Hu, M., Wang, H., Lou, S., Li, J., Sun, J., Li, X. and Sheng, L.,: Modeling particulate nitrate in China: Current findings and future directions, Environment International, 166, 107369, https://doi.org/10.1016/j.envint.2022.107369, 2022.
 - Yienger, J. J. and Levy, H.: Empirical model of global soil-biogenic NOx emissions, Journal of Geophysical Research: Atmospheres, 100, 11447-11464, https://doi.org/10.1029/95JD00370, 1995.
 - Yu, X. Y., Lee, T., Ayres, B., Kreidenweis, S. M., Collett, J. L., & Malm, W.: Particulate Nitrate Measurement Using Nylon Filters, Journal of the Air & Waste Management Association, 55, 1100–1110. https://doi.org/10.1080/10473289.2005.10464721, 2005.
 - Zakoura, M. and Pandis, S. N.: Overprediction of aerosol nitrate by chemical transport models: The role of grid resolution, Atmospheric Environment, 187, 390-400, https://doi.org/10.1016/j.atmosenv.2018.05.066, 2018.
 - Zakoura, M., & Pandis, S. N.: Improving fine aerosol nitrate predictions using a Plume-in-Grid modeling approach, Atmospheric Environment, 215, 116887, https://doi.org/10.1016/j.atmosenv.2019.116887, 2019.
- Zhang, X., Wu, Y., Liu, X., Reis, S., Jin, J., Dragosits, U., Van Damme, M., Clarisse, L., Whitburn, S., Coheur,
 P.F. and Gu, B.,: Ammonia emissions may be substantially underestimated in China,

https://doi.org/10.5194/egusphere-2025-313 Preprint. Discussion started: 12 February 2025 © Author(s) 2025. CC BY 4.0 License.





1383	Environmental Science & Technology, 51, 12089-12096, https://doi.org/10.1021/acs.est.7b02171	
1384	, 2017.	
1385		